

bradscholars

Maximization of gasoline in an industrial FCC unit

Item Type	Article
Authors	John, Yakubu M.;Patel, Rajnikant;Mujtaba, Iqbal
Citation	John YM, Patel R and Mujtaba IM (2017) Maximization of gasoline in an industrial FCC unit. Energy and Fuels. 31(5): 5645-5661.
DOI	https://doi.org/10.1021/acs.energyfuels.7b00071
Rights	© 2017 American Chemical Society. This document is the Accepted Manuscript version of a Published Work that appeared in final form in Energy and Fuels, copyright © American Chemical Society after peer review and technical editing by the publisher. To access the final edited and published work see http://dx.doi.org/10.1021/acs.energyfuels.7b00071
Download date	2025-04-28 12:01:27
Link to Item	http://hdl.handle.net/10454/11746

The University of Bradford Institutional Repository

<http://bradscholars.brad.ac.uk>

This work is made available online in accordance with publisher policies. Please refer to the repository record for this item and our Policy Document available from the repository home page for further information.

To see the final version of this work please visit the publisher's website. Access to the published online version may require a subscription.

Link to publisher's version: <http://dx.doi.org/10.1021/acs.energyfuels.7b00071>

Citation: John YM, Patel R and Mujtaba IM (2017) Maximization of gasoline in an industrial FCC unit. *Energy and Fuels*. 31(5): 5645-5661.

Copyright statement: © 2017 American Chemical Society. This document is the Accepted Manuscript version of a Published Work that appeared in final form in *Energy and Fuels*, copyright © American Chemical Society after peer review and technical editing by the publisher. To access the final edited and published work see <http://dx.doi.org/10.1021/acs.energyfuels.7b00071>

1 Maximization of Gasoline in an Industrial FCC Unit

2 Yakubu M. John, Raj Patel, Iqbal M. Mujtaba*

3 *Chemical Engineering Division, School of Engineering, Faculty of Engineering and*
4 *Informatics, University of Bradford, Bradford, BD7 1DP, UK*

5 * I.M.Mujtaba@bradford.ac.uk

7 Abstract

8 The Riser of a Fluid Catalytic Cracking (FCC) unit cracks gas oil to make fuels such as
9 gasoline and diesel. However, changes in quality, nature of crude oil blends feedstocks,
10 environmental changes and the desire to obtain higher profitability, lead to many alternative
11 operating conditions of the FCC riser. The production objective of the riser is usually the
12 maximization of gasoline and diesel. Here, an optimisation framework is developed in
13 gPROMS to maximise the gasoline in the riser of an industrial FCC unit (reported in the
14 literature) while optimising mass flowrates of catalyst and gas oil. A detailed mathematical
15 model of the process developed is incorporated in the optimisation framework. It was found
16 that, concurrent use of the optimal values of mass flowrates of catalyst (310.8 kg/s) and gas
17 oil (44.8 kg/s) gives the lowest yield of gases, but when these optimum mass flowrates are
18 used one at time, they produced the same and better yield of gasoline (0.554 kg lump/ kg
19 feed).

20 Keyword: FCC Riser; Modelling; Gasoline maximization; Optimization

22 1. Introduction

23 The FCC unit is known in modern refineries for making treasured transportation fuels such as
24 gasoline and diesel. It also serves as the source of feedstocks for the main downstream
25 processes that also contribute to the gasoline pool ¹. Gasoline and diesel are fuels produced
26 by many processes in the downstream sector of the petroleum industry; however, not all
27 processes are as good as using the FCC unit to meet the high demand for fuels. For instance,
28 a typical barrel of crude is approximately 20% straight run gasoline, but demand is nearly
29 50% per barrel which can be met using an efficient FCC unit. This could be achieved by
30 using the riser to crack gas oil (mostly a product of the atmospheric and vacuum distillation
31 unit) into lighter hydrocarbons such as gasoline.

32 The riser is a hollow cylinder capable of generating high yields of gasoline, liquefied
33 petroleum gas (LPG) and other intermediate products such as light cycle oil (LCO) if suitable
34 operating conditions are used. It has a very high profitability and hence operate at maximum
35 capacity, that is, maximum feed rate and maximum power applied to auxiliary equipment like
36 the gas compressor and air blower drivers ². However, optimal operating conditions of an
37 FCC riser required to operate at the maximum capacity of the plant change with the changes
38 in quality and nature of blends of the feedstock ². Other issues that affect the operating
39 conditions can be environmental changes and the desire to make large profits via increased
40 production of gasoline by cracking the various intermediate fractions into gasoline or by
41 converting the gasoline fractions into LPG.

42 The riser is a complex unit due to its multivariable nature, nonlinear features, complex
43 dynamics, severe operating restrictions and strong interactions among the process variables.
44 These pose a challenging optimization problem, though, even little improvements in the
45 optimal operation of the riser can lead to large economic benefits ³⁻⁴. Also, due to the
46 complex nature of the processes involved in the FCC unit, there is not yet an answer to the
47 question of how best to operate it ³⁻⁴. Any attempt to optimize the riser is an attempt to
48 establish the best operational route for the unit and that is what this work sets to achieve.

49 Many optimization studies have been carried out on the FCC unit and presented in the
50 literature, some of them used single objective function ⁵. Other techniques used to set optimal
51 operating conditions for the FCC unit are the Genetic Algorithm (GA) and Particle Swarm
52 Optimization (PSO) evolutionary methods. Both algorithms gave good and consistent results
53 for typical FCC optimization problems ⁶.

54 In obtaining solutions to the optimization problems, some of the techniques used required the
55 writing of codes for complex model equations, but it is time consuming and not void of error.
56 Sometimes, having oversimplified models limit the accuracy of results. To eliminate this
57 challenge, a fast and sufficiently precise model, not too simplified, is required for
58 optimization. According to Souza et al.,⁷ an adequate model used for optimization should
59 have a fast and sufficiently precise code that can be used to run several simulations (each one
60 for a specific operating condition) and be able to search for the best values for the input
61 variables (mass concentrations, temperatures, etc.). This however is a difficult balance (i.e., a
62 fast and sufficiently precise model) ⁷. The model used by Han et al.¹⁰ for optimization and the
63 model used in this work is a one-dimensional momentum, energy and mass balance model

64 and was taken from the literature ⁸⁻⁹. Although, Han et al.¹⁰ further revised or simplified the
65 model of the riser to support their optimization studies ¹⁰, the original model ⁸⁻⁹ is used in this
66 optimization study without being simplified as gPROMS (software used in this work) can
67 handle complex models for simulation and optimisation. A one-dimensional momentum,
68 energy and mass balance model was considered to be adequate for optimization studies
69 because it is able to predict the overall performance of the FCC riser unit ¹¹. Hence, the
70 model used in this optimization study is deemed adequate for riser optimization. This study is
71 an attempt to improve the profitability of the FCC unit, by maximizing the yield of gasoline
72 in a single objective function while optimizing the operating variables of the riser. gPROMS
73 uses a successive reduced quadratic programming (SRQPD), a Sequential Quadratic
74 Programming based solver to maximize the yield of gasoline in the riser. The optimization
75 results were compared with the data in several open-literatures ⁸⁻¹⁰.

76

77 **Process Modelling**

78 This section presents the description of the riser and its model assumptions, the model
79 equations, degree of freedom analysis, the parameters used and the development of the
80 optimization model.

81

82 **The Riser**

83 The riser in a FCC unit is a single vertical tube as shown in Figure 1. It is modelled as a one-
84 dimensional plug flow reactor without axial and radial dispersion. It is a 30 m height riser and
85 1.1 m diameter. Other specifications of the riser is found in the Appendix Table A.3.

86 The momentum, mass and energy balance equations for the catalyst and gaseous phases are
87 obtained under the following assumptions:

- 88 1. The hydrocarbon feed instantly vaporizes as it comes into contact with the hot catalyst
89 from the regenerator, then moves upwards in thermal equilibrium with the catalyst
90 and there is no loss of heat from the riser ¹².
- 91 2. The cracking reactions only take place in the riser, on catalyst surface and fast enough
92 to justify steady state model.
- 93 3. The vaporization section of the riser was not considered in the simulation.
- 94 4. The rates of dispersion and adsorption inside the catalyst particles are negligible.

95

96

97

98

99

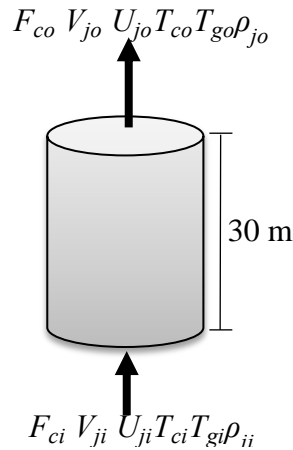
100

101

102

103

104



105

Figure 1: The Riser in a FCC

106

107

108

109

110

111

112

At the entrance of the riser, the feed vaporizes immediately and it comes in contact with the regenerated catalyst and flows pneumatically upwards in the riser as cracking goes along on the surface of the catalyst to form products. The products in this case are gasoline, gases and coke, based on the four lumped model. The four lumped kinetic model used in this study was obtained from the literature ¹³ and is presented in Figure 2. It represents gas oil as the reactant while gasoline, gases and coke as products.

113

114

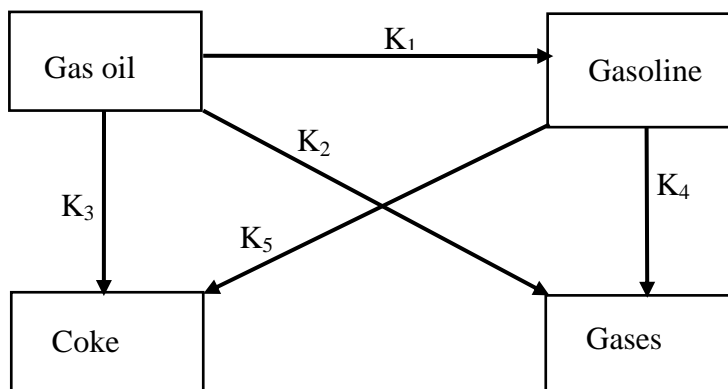
115

116

117

118

119



120

Figure 2: Four-lumped model of gas oil cracking reactions ¹³.

121

122

123

124

125

To produce a kinetic model which captures all chemical reactions involved in the cracking of gas oil is extremely difficult ¹⁴⁻¹⁵. Hence, most researchers group the reactant and products into valuable lumps. The kinetic model shown in Figure 2 is the breaking down of gas oil into gases, coke and gasoline. It is the most acceptable and widely used because it considers the

126 important refinery fractions ¹⁶. The cracking reaction is endothermic and the heat required for
 127 the endothermic reaction comes from catalyst regeneration. Thus, there is the need to
 128 accurately predict the amount of coke formed due to catalyst deactivation. The coke formed
 129 aids heat integration and reactor temperature control which is one of the advantages of the
 130 four-lump model ⁸.

131 In Figure 2, K_1 , K_2 , K_3 , K_4 and K_5 are the overall rate constants for the cracking reactions.
 132 The order of reaction and path taken are shown in Table 1, while their kinetic parameters are
 133 presented in Table A.3. The cracking of gas oil to form gasoline, gases and coke is
 134 considered to be a second order reaction, while the cracking of gasoline to form gases and
 135 coke is considered a first order reaction.

136

137 Table 1: Four lump cracking of gas oil ⁹

4-lump cracking reactions	Reaction Path	Order of reaction
Gas oil – Gasoline	1	2
Gas oil –C ₁ -C ₄ gases	2	2
Gas oil- Coke	3	2
Gasoline–C ₁ -C ₄ gases	4	1
Gasoline- Coke	5	1

138

139 **Model Equations**

140 The model equations along with their parameters and feed conditions used in this
 141 optimization study were adopted from literature ⁸⁻⁹. Although, the same model was used by
 142 Han et al. ¹⁰ for optimization study, there are many differences which are highlighted below:

143 Han et al. ¹⁰ replaced the riser momentum equations of Han and Chung ⁸ with simple linear
 144 correlation equations. In this study the riser momentum equations have been retained. Han et
 145 al. ¹⁰ merged the two-phase (gas and solid) energy balance equations of the riser ⁸ into a
 146 single-phase balance in their process model for optimization study. In this study, the two-
 147 phase energy balance equations are retained in the model. Han and Chung ⁸ used the 4-
 148 lumped kinetic model for simulation while Han et al. ¹⁰ used a 10 lumped kinetic model for
 149 optimisation. This study used the 4-lumped kinetic model which cracks gas oil into gasoline,
 150 gases and coke as explained earlier. In the event that gasoline and coke are the most
 151 important products of the riser, the 4-lumped model is suitable over any lumped model. More
 152 suitable than the 3-lumped model because the 3-lumped model has no coke as a lump which

153 is useful for the heat integration in the FCC unit. The coke is burnt to generate the
 154 endothermic heat required for the cracking reactions in the riser, hence the usefulness of the
 155 4-lumped model. Other lumped models including the 10-lumped model are suitable in the
 156 event that the subdivisions of fractional yields are needful ⁸. The 10-lumped model as well
 157 produces the coke as a lump but the interest is more than just gasoline and coke. However, in
 158 this optimization study, the 4-lumped is adequate because the interest is just the yield of
 159 gasoline. This informed the use of 4-lumped model in this work. Another reason for use of
 160 the 4-lumped model was for effective comparison of this simulation work with that of the
 161 Han and Chung ⁸ which used 4-lumped model. Also, Han et al. ¹⁰ converted all the differential
 162 equations of their steady-state process model to algebraic equations by discretizing the spatial
 163 derivatives of the equations using backward finite differences. This study does not require
 164 such discretisation as gPROMS is capable of handling complex systems differential and
 165 algebraic equations (DAEs) directly.

166

167 The riser shown in Figure 1 is modelled as a one-dimensional tubular reactor using
 168 momentum, mass and energy balance equations. The one-dimensional homogeneous plug-
 169 flow model is simple and can house a huge number of about 30,000 reactions involving about
 170 3000 reacting species, which is not the case with multi-dimensional flow models like the
 171 CFD system where chemical reactions is necessarily small ¹⁷. In spite the simplicity of the
 172 one-dimensional models, a detailed three-dimensional two-phase modelling study was carried
 173 out to study the flow patterns and heat transfer in FCC riser and was concluded that the
 174 overall performance of the riser can be predicted using this simple one-dimensional total
 175 mass, energy, and chemical species balances ¹¹. The following equations in this section
 176 (Equations (1-31)) and those in the Appendix (Equations (A.1 – A.34)), which are mostly
 177 correlations were all used in this simulation. Equations 1 and 2 are derived from the energy
 178 balance of the riser showing the temperature of catalyst and gas phases respectively:

179

$$180 \quad \frac{dT_c}{dx} = \frac{\Omega h_p A_p}{F_c C_{pc}} (T_g - T_c) \quad (1)$$

$$181 \quad \frac{dT_g}{dx} = \frac{\Omega}{F_g C_{pg}} [h_p A_p (T_c - T_g) + \rho_c \epsilon_c Q_{react}] \quad (2)$$

182 The material balance for the reaction showing the four lumps; gas oil, gasoline, light gas and
 183 coke are given respectively as Equations (3 - 6):

$$184 \quad \frac{dy_{go}}{dx} = \frac{\rho_c \epsilon_c \Omega \theta_c}{F_g} R_{go} \quad (3)$$

$$185 \quad \frac{dy_{gl}}{dx} = \frac{\rho_c \varepsilon_c \Omega \phi_c}{F_g} R_{gl} \quad (4)$$

$$186 \quad \frac{dy_{gs}}{dx} = \frac{\rho_c \varepsilon_c \Omega \phi_c}{F_g} R_{gs} \quad (5)$$

$$187 \quad \frac{dy_{ck}}{dx} = \frac{\rho_c \varepsilon_c \Omega}{F_g} R_{ck} \quad (6)$$

188 The rates of reaction for gas oil R_{go} , gasoline R_{gl} , light gas R_{gs} , and coke R_{ck} , are given as

$$189 \quad R_{go} = -(K_1 + K_2 + K_3)y_{go}^2 \quad (7)$$

$$190 \quad R_{gl} = (K_1 y_{go}^2 - K_4 y_{gl} - K_5 y_{gl}) \quad (8)$$

$$191 \quad R_{gs} = (K_2 y_{go}^2 - K_4 y_{gl}) \quad (9)$$

$$192 \quad R_{ck} = (K_3 y_{go}^2 - K_5 y_{gl}) \quad (10)$$

193 The rate constants K_i , of reaction path $i = 1$ to 5 and their corresponding frequency factors k_{i0}
194 are given as:

$$195 \quad K_1 = k_{10} \exp\left(\frac{-E_1}{RT_g}\right) \quad (11)$$

$$196 \quad K_2 = k_{20} \exp\left(\frac{-E_2}{RT_g}\right) \quad (12)$$

$$197 \quad K_3 = k_{30} \exp\left(\frac{-E_3}{RT_g}\right) \quad (13)$$

$$198 \quad K_4 = k_{40} \exp\left(\frac{-E_4}{RT_g}\right) \quad (14)$$

$$199 \quad K_5 = k_{50} \exp\left(\frac{-E_5}{RT_g}\right) \quad (15)$$

200 Q_{react} is the rate of heat generation or heat removal by reaction and can be written as

$$201 \quad Q_{react} = -(\Delta H_1 K_1 y_{go}^2 + \Delta H_2 K_2 y_{go}^2 + \Delta H_3 K_3 y_{go}^2 + \Delta H_4 K_4 y_{gl} + \Delta H_5 K_5 y_{gl}) \phi_c \quad (16)$$

202 The gas volume fraction, ε_g , and catalyst volume fraction, ε_c , can be obtained from:

$$203 \quad \varepsilon_g = 1 - \varepsilon_c \quad (17)$$

204 The catalyst volume fraction, ε_c , can be obtained from:

$$205 \quad \varepsilon_c = \frac{F_c}{v_c \rho_c \Omega} \quad (18)$$

206 The cross sectional area of the riser, Ω , is given as:

$$207 \quad \Omega = \frac{\pi D^2}{4} \quad (19)$$

208 The effective interface heat transfer area per unit volume between the catalyst and gas phases,

$$209 \quad A_{ptc} = \frac{6}{0.72 d_c} * (1 - \varepsilon_g) \quad (20)$$

210 The catalyst deactivation is given by:

$$211 \quad \phi_c = \exp(-\alpha_c C_{ck}) \quad (21)$$

212 Where;

$$213 \quad \alpha_c = \alpha_{c0} \exp\left(\frac{-E_c}{RT_g}\right) (R_{AN})^{\alpha_{c*}} \quad (22)$$

214 and

$$215 \quad C_{ck} = C_{ckCL1} + \frac{F_g y_{ck}}{F_c} \quad (23)$$

216 The density of the gas phase is given by:

$$217 \quad \rho_g = \frac{F_g}{\varepsilon_g v_g \Omega} \quad (24)$$

218 The riser pressure is given by:

$$219 \quad P = \rho_g \frac{RT_g}{M_{wg}} \quad (25)$$

220 The ratio of the mass flowrate of catalyst to the mass flowrate of gas oil is catalyst-to-oil ratio
221 (C/O) ratio and it is given by:

$$222 \quad C/O \text{ ratio} = \frac{F_c}{F_g} \quad (26)$$

$$223 \quad T_{pr} = \frac{T_g}{T_{pc}} \quad (27)$$

$$224 \quad P_{pr} = \frac{P}{P_{pc}} \quad (28)$$

225 The momentum balance equations gives catalyst and gas velocity distribution across the riser
226 as :

$$227 \quad \frac{dv_c}{dx} = - \left(G_c \frac{\Omega}{F_c} \frac{d\varepsilon_c}{dx} - \frac{C_f(v_g - v_c)\Omega}{F_c} + \frac{2f_{rc}v_c}{D} + \frac{g}{v_c} \right) \quad (29)$$

$$228 \quad \frac{dv_g}{dx} = - \left(\frac{\Omega}{F_g} \frac{dP}{dx} - \frac{C_f(v_c - v_g)}{F_g} + \frac{2f_{rg}v_g}{D} + \frac{g}{v_g} \right) \quad (30)$$

229 The stress modulus¹⁸ of the catalyst is calculated by:

$$230 \quad G_c = 10^{(-8.76\varepsilon_g + 5.43)} \quad (31)$$

231 The entire DAE model equations can be written in compact form as:

$$f(x, z'(x), z(x), u(x), v) = 0$$

232 Where x is the independent variable (height of riser), $z(x)$ the set of all state variables, $z'(x)$
233 the derivatives of $z(x)$ with respect to the height of the riser, $u(x)$ the vector of control
234 variables (mass flowrates of feed and catalyst) and v a vector of invariant parameters, such
235 as design variables (riser diameter and height).

236

237 **Degree of Freedom Analysis**

238 The analysis for the degree of freedom of the model equations is shown in Table A.1
239 (Appendix A). The model equations are made up of eight (8) ordinary differential equations
240 (ODEs) and fifty-one (51) algebraic equations (AEs), making a total of fifty-nine (59)
241 equations as shown in Tables A.1. The riser model contains one hundred and twenty-one
242 (121) variables as shown in Table A.2.

243 Degree of freedom (DF) = Total number of variables – Total number of equation
244 $Df = 121 - 59 = 62$. Hence, eight initial conditions for the differential variables are
245 assigned along with fifty-three parameters (Table A3), and one independent variable, x .

246

247 **Optimization Problem Formulation**

248 In the past different modelling and optimisation platform/software such as Matlab and Hysys
249 were used for FCC simulation/optimisation but only little with gPROMS ¹⁹, in spite of its
250 robustness. In this work gPROMS is used for the riser optimisation.

251 Several FCC models have been proposed in the literature for the optimization of FCC units ¹⁰,
252 ²⁰⁻²¹. Most of the optimizations were based on the maximization of the production of products
253 with economic objectives, where the best operating conditions (e.g., mass flows, inlet
254 temperatures) were determined for the maximum performance ⁷. In this study maximisation
255 of gasoline product is considered.

256

257 The optimization problem can be described as:

258	Given	the fixed volume of the riser
259	Optimize	the mass flowrate of catalyst, mass flowrate of gas oil and 260 temperature profiles of gas phase and catalyst.
261	So as to maximize	the yield of gasoline
262	Subject to	constraints on the mass flowrates of catalyst and gas oil, 263 temperatures of gas phase and catalyst, exit concentrations of 264 gases and coke.

265

266 Mathematically, the optimization problem can be written as;

267 $\max_{T(x) \text{ or } F_j(x)} Z$

268 (32)

269 *s. t.*

270 $f(x, z'(x), z(x), u(x), v) = 0$ (model equations) (33)

271 $x_f = x_f^*$ (34)

272 $T_L \leq T \leq T_U$ or $F_L \leq F \leq F_U$ (35)

273 $Y_{CD} < Y_{CD}^*$ (36)

274

275 Where Z is the yield of gasoline, the desired product in the riser, T the catalyst and gas phase
 276 temperature, F_j the mass flow rates of catalyst and gas oil, x_f the height of the riser, Y_{CD} the
 277 yield of gases and coke, T_L and T_U the lower and upper bounds of the catalyst phase
 278 temperature ($788 \leq T_c \leq 933 K$) and gas phase temperature ($785 \leq T_g \leq 795 K$)
 279 respectively, F_L and F_U the lower and upper bounds of the mass flowrate of catalyst ($200 \leq$
 280 $F_{cat} \leq 500 \frac{kg}{s}$) and mass flowrate of gas oil ($20 \leq F_g \leq 100 \frac{kg}{s}$) respectively, x_f^* the fixed
 281 height of the riser and Y_{CD}^* the maximum allowable limit for gases $Y_C < 0.2$ and coke
 282 $Y_D < 0.1$.

283 In choosing the upper and lower limits of the decision variables, it is well-known that
 284 temperature of the reacting phases in the riser and catalyst-to-feed flow ratio, C/O are the
 285 dominant cracking intensity indicators¹⁷, they are strong determinants of conversion of
 286 feedstock and yield of products²². Hence, the temperatures and mass flowrates of the
 287 catalyst and gas oil were chosen as the decision variables. And for the choice of the upper and
 288 lower limits for the decision variables, depending on the feed preheat, regenerator bed, and
 289 riser outlet temperatures, the ratio of catalyst to oil is normally in the range of 4:1 to 10:1 by
 290 weight²³⁻²⁴. Therefore, the lower and upper bounds of the catalyst flow rate and the feed flow
 291 rate which makes the catalyst-to-feed flow ratio, C/O were chosen to lie between 4 and 10.1
 292 at all points during the optimization run. Below and above these ratios, unnecessary steady
 293 states occurs that have no relevance in industrial operations. In addition, the upper limit of the
 294 feed temperature and lower limit of the catalyst temperature were chosen in order to avoid the
 295 production of more coke, more gases and promote secondary reactions of gasoline. For the
 296 same reason the lower limit of the temperature of the catalyst phase was chosen.

297

298 **Results and Discussions**

299 This section presents both simulation results and optimization results. The purpose of
 300 presenting the simulation results is to demonstrate the capability of gPROMS in solving

301 complex nonlinear DAEs by validating the results against those predicted by the same model
302 but using different solution software as DSim-FCC⁹.

303

304 Simulation

305 When gas oil comes in contact with the catalyst, it begins to crack to form cracked lumps;
306 gasoline, gases and coke. In this study, the cracking reaction is set to take place at gas oil
307 inlet temperature of 535 K and the inlet temperature of catalyst at 933 K. The profiles of the
308 products are presented in Figure 3.

309

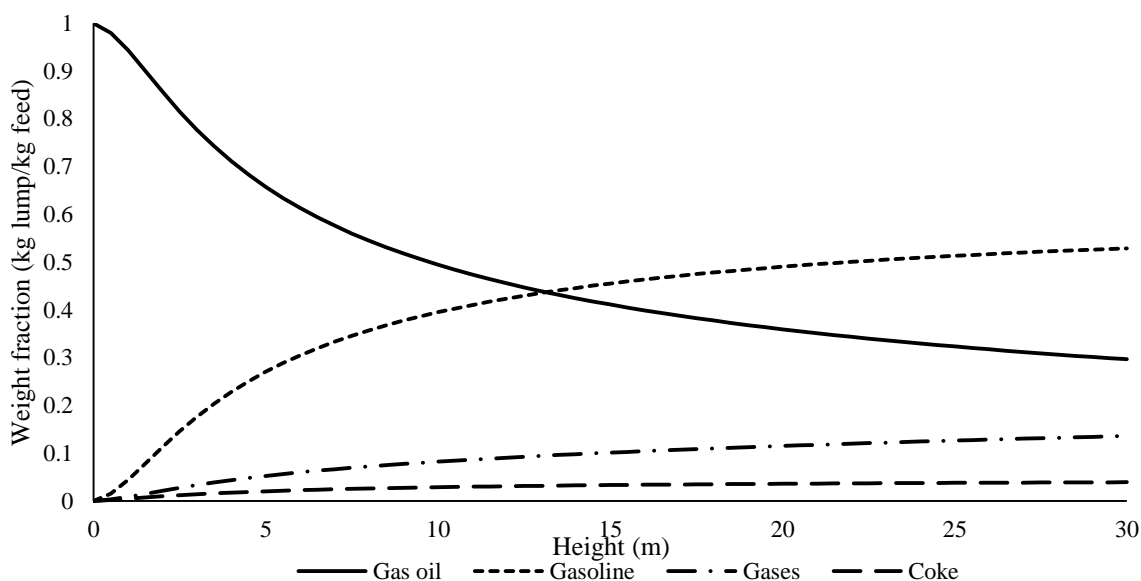


Figure 3: Base case steady-state lumps profiles along the riser

310

311

312 The fraction of the gas oil at the exit of the riser is 0.296 (kg lump/kg feed) which is 29.6% of
313 gas oil left unconverted. It also means, about 70.4% of gas oil was consumed and 70% of the
314 fraction is consumed in the first 14 m of the riser. In Han and Chung,⁹ the fraction of gas oil
315 at the exit of the riser is 0.276 (kg lump/kg feed) which corresponds to 72.4% of gas oil
316 consumed. This difference can be caused by the assumption in this study of using
317 instantaneous vaporization of gas oil. This explains the reason for some differences which
318 can be noticed for the other lumps; gasoline, gases and coke at the exit of the riser for this
319 study and that of Han and Chung.⁸ The gasoline profile increases nonlinearly from 0 (kg
320 lump/kg feed) at the inlet of the riser to its maximum yield of 0.529 (kg lump/kg feed) and
321 essentially levels out at the exit of the riser. The catalytic cracking of gas oil is a multiple
322 reaction²⁵, and gasoline being an intermediate is expected to rise to a maximum and then fall
323 due to a secondary reaction as seen in Figure 3. The yield almost compares favorably with

324 the value of about 51.2 wt% obtained by Han and Chung.⁹ The coke concentration increases
 325 nonlinearly from 0 (kg lump/kg feed) at the inlet to 0.039 (kg lump/kg feed) at the exit of the
 326 riser. Coke concentration at the riser exit from Han and Chung⁹ is 0.047 (kg lump/kg feed).
 327 The yield of the gases increases nonlinearly from 0 (kg lump/kg feed) at the inlet of the riser
 328 to a maximum of 0.136 (kg lump/kg feed) at the exit. The concentration of gases at the riser
 329 exit from Han and Chung⁹ is 0.142 (kg lump/kg feed). The profile of gases and coke in this
 330 work compares qualitatively well with the validated results obtained by Han and Chung⁹
 331 where the same model was adopted.

332 Figure 4 shows the temperature profiles of the gas and catalyst phases as a function of riser
 333 height at base case condition (simulation). The temperature of the catalyst-phase starts from
 334 about 933 K and decreases for the first 8 m and then essentially levels out. The temperature
 335 profile of the gas phase starts from about 535 K and rises to a peak in the first 6 m of the riser
 336 and levels out for the remaining portion of the riser. Both profiles came so close to the same
 337 value with temperature difference of about 1 °C which is necessary for the completion of the
 338 reaction. The temperature profiles obtained in this work are similar to those obtained in many
 339 literatures^{9, 12, 26}.

340

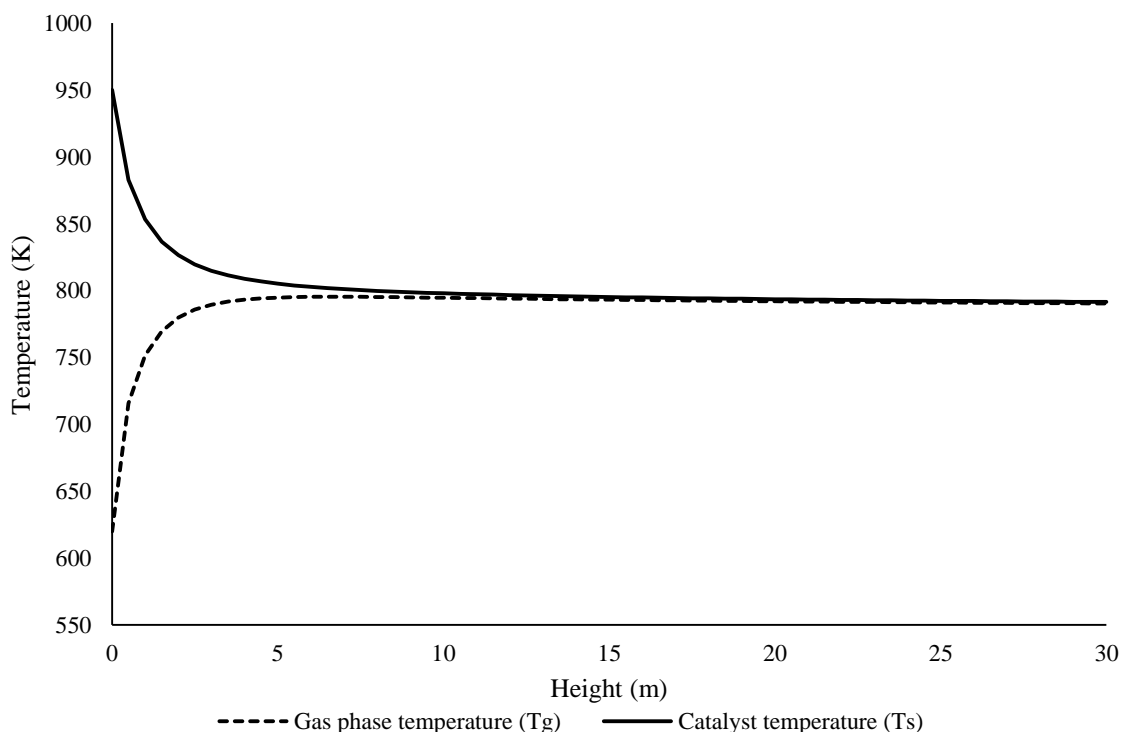


Figure 4: Base case temperature profile along the riser

341

342 Figure 5 shows the velocity profiles (gas and catalyst phases) along the riser height at base
 343 case conditions. Both the catalyst and gas velocities rise relatively sharply from about 10 m/s

344 at the riser bottom to about 33 m/s at the exit of the riser. As the gas oil vaporizes, the slip
345 velocity between the two phases is maintained within 0.25 m/s. The slip velocity is similar to
346 the one obtained by Han and Chung.⁹

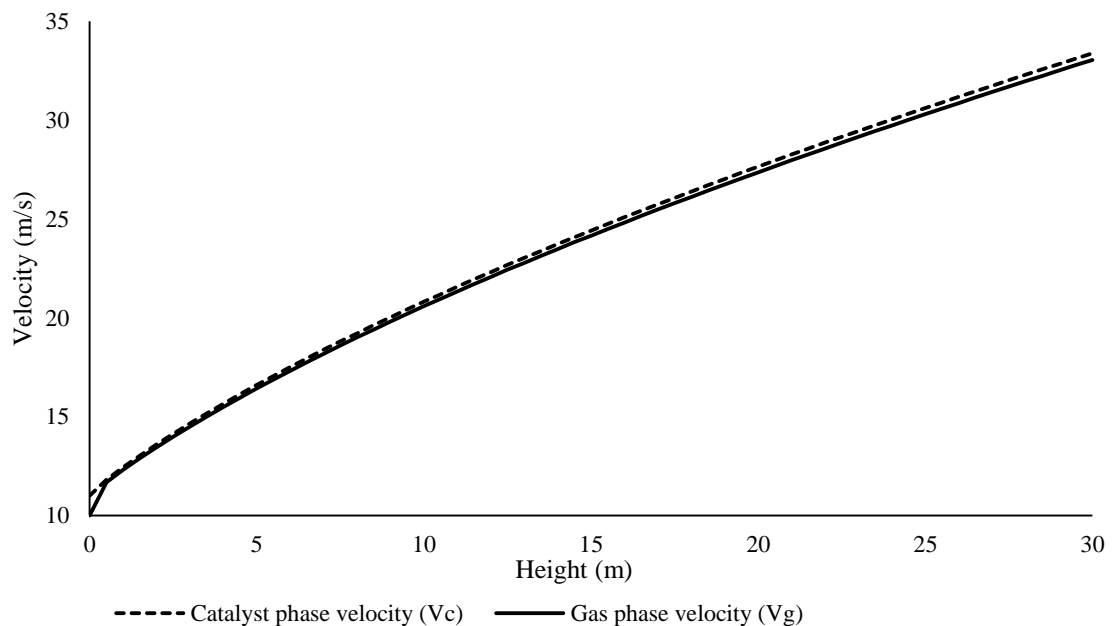


Figure 5: Riser base case steady-state velocity profile

347
348 Figure 6 shows the pressure profiles in the riser. The total pressure drop is 54.83 kPa for the
349 base case response, which is not consistent with 16 kPa, obtained by Han and Chung.⁹ This
350 could be due to the fact that the vaporization section model was not considered in this work.
351 The vaporization section vaporizes the feed using steam, which is a major contributor of the
352 pressure differential in the riser. Where there is limited steam supply, the pressure drop is
353 high²⁷, which explains the reason for the high pressure drop observed in this simulation.
354 Though, the velocities and pressure profiles are quantitatively different from the validated
355 results obtained by Han and Chung⁹ they are qualitatively similar.

356

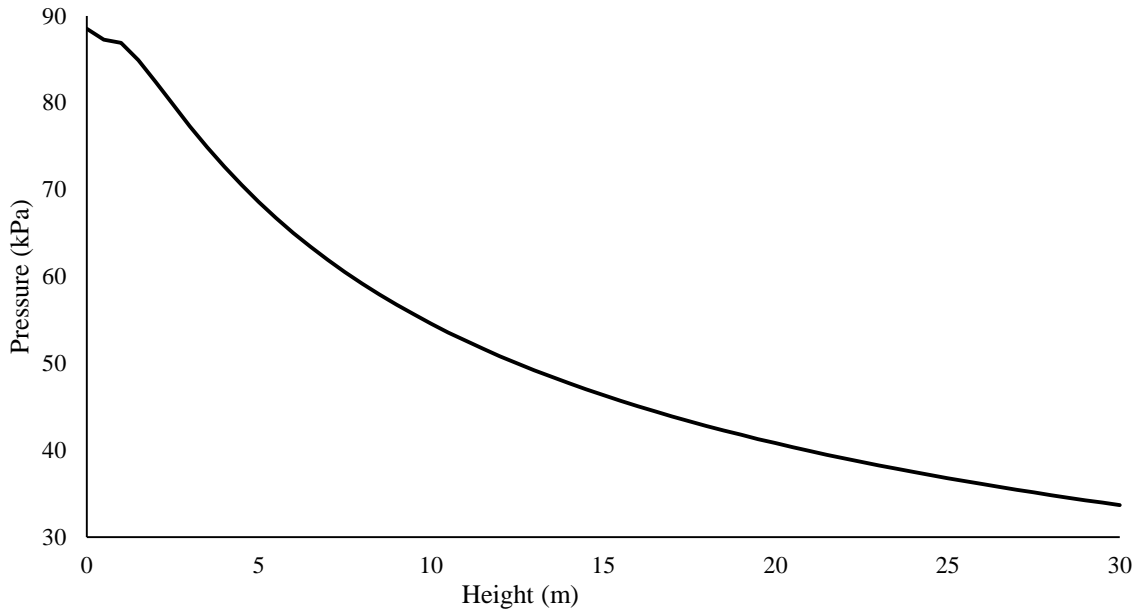


Figure 6: Base case pressure profile along the riser

357

358

359 To determine the accuracy and validate the capability of this gPROMS model, results from
 360 validated work of Han and Chung⁸⁻⁹ shown in column B of Table 2, and Kaduna refinery
 361 operational data shown in column C, are used to compared with the results of this simulation
 362 work. The results are presented in Table 2.

363

364 Table 2: Compare Riser output results with other simulation and plant data

Parameter	Input	Riser output				
		A	B	C	% Deviation	
					A with B	A with C
Gas Oil Temperature (K)	535	790.4	793.1	800	-0.34	-1.21
Catalyst Temperature (K)	933	791.5	796.5		-0.63	
Gas Oil Mass flowrate (kg/s)	49.3	49.3	49.3			
Catalyst Mass flowrate (kg/s)	300	300	300			
Mass fraction of Gas Oil	1	0.296	0.273	0.236	7.77	20.27
Mass fraction of Gasoline	0	0.529	0.514	0.515	2.83	2.64
Mass fraction of Gases	0	0.136	0.136	0.198	0	-45.58
Mass fraction of Coke	0	0.039	0.042	0.051	-7.69	-30.76

365

366 The experimental data for comparing this gPROMS model quantitatively and qualitatively
 367 are the validated results from Han and Chung⁸⁻⁹ models where the gPROMS model used in

368 this work was obtained. Han and Chung⁸⁻⁹ simulation results were validated against plant
369 and literature data, which makes it suitable to be referenced. In addition, yields from the riser
370 are functions of the feed quality, catalyst type, reaction temperature, catalyst to oil ratio and
371 many other operational variables. Since, the input conditions, including the feed quality,
372 catalyst type, reaction temperature, catalyst to oil ratio and riser configuration for Han and
373 Chung⁸⁻⁹ and this simulation are the same, this simulation results are compared with that of
374 Han and Chung.⁸⁻⁹ And it shows from Table 2 that, percentage deviation (column A with B)
375 between the results of this simulation (column A) and the Han and Chung⁸⁻⁹ (column B) are
376 within a marginal error of less than 3 %, except for mass fractions of gas oil and coke which
377 are about +7.77 and -7.69 respectively. This shows that the gPROMS is accurate in predicting
378 the results obtained by Han and Chung⁸⁻⁹ and can be recommended for the simulation of the
379 FCC unit as a whole. The percentage deviation (column A with C) between the results of this
380 simulation (column A) and the plant data (column B) are quite wide mainly due to
381 differences in the feed quality, catalyst type, reaction temperature, catalyst to oil ratio and
382 many other operational variables. The C/O in this simulation is 6.085, while for the data
383 obtained from Kaduna refinery, C/O is 7.0. However, the fractional yield of gasoline for this
384 model is 0.529, while for the plant is 0.515, which is a percentage difference of 2.64 and it is
385 within the reasonable limit of acceptability. The fractional yield of gasoline in this work is
386 better than that of Han and Chung⁸⁻⁹ and better than that of the plant data as well, hence,
387 optimal yield of gasoline for the optimization cases carried out in this work will only be
388 compared with the yield of gasoline from Han and Chung⁸⁻⁹ where the model of this work
389 was obtained. Many literatures however show that the profiles the yields of gas oil, gasoline,
390 gases, coke and temperatures obtained from this gPROMS simulation are qualitatively
391 consistent^{16,28}.

392

393 **Optimization**

394 The optimization results for this work are presented in Figures (7 to 14). Figure 7 shows the
395 profiles of the four lumps; gas oil as feed while gasoline, gases and coke as products at both
396 base case conditions and optimized conditions for case 1. It compares the optimized case 1
397 with the base case simulation results. The base case simulation was also presented earlier to
398 allow a comparison of before and after optimisation. The system was set at gas-oil
399 temperatures of 535 K and catalyst temperature of 933 K. The gas-oil and catalyst velocities
400 were set at the inlet of the riser at 10 m/s and 11 m/s respectively. The vaporization of gas oil
401 was considered to be instantaneous and hence the vaporization section was neglected.

402 In the optimisation case 1, the decision variable (catalyst flow rate) was set to be optimized
 403 between 100 kg/s to 500 kg/s, while the gas oil mass flow rate, gas-oil and catalyst
 404 temperatures were fixed at 49.3 kg/s, 535 K and 933 K respectively.

405

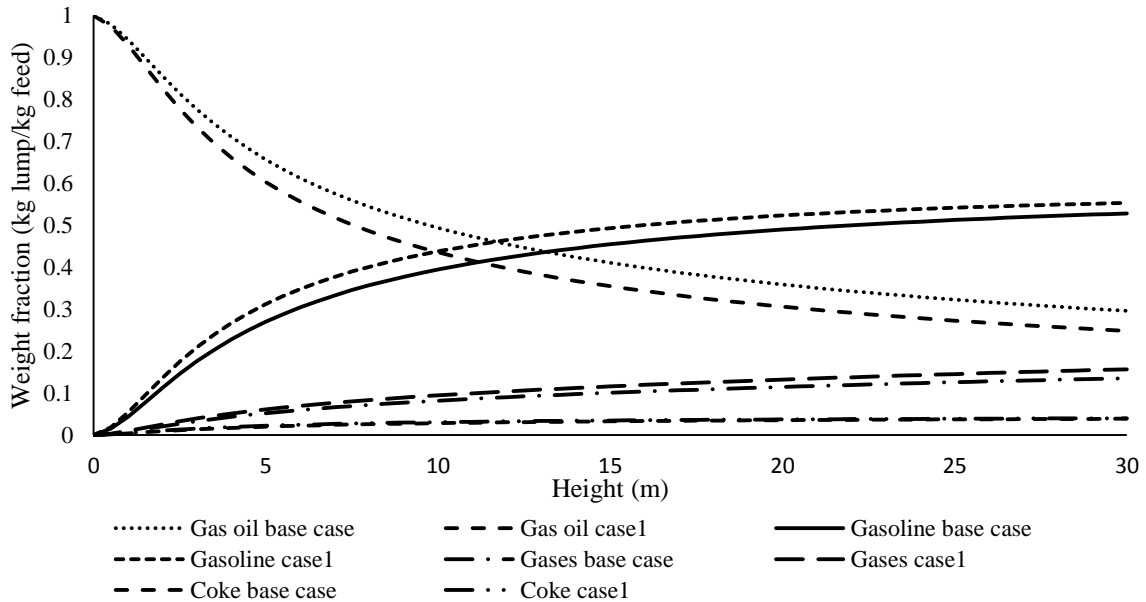


Figure 7: Four lump profile base and optimized cases 1

406

407

408 The unconverted gas oil in the base case condition is 0.296 kg-lump/kg-feed which is about
 409 70.40% conversion while the unconverted for the optimized case 1 is 0.249 kg-lump/kg-feed.
 410 This is a difference of 6.26% increased conversion corresponding to 75.10% conversion of
 411 gas oil and resulted in 4.51%, 13.54% and 2.50% increase in gasoline, gases and coke
 412 respectively.

413 Table 3 shows the exit mass fractions and operating conditions for the base case and
 414 optimized case 1. The percentage increase shown in Tables 3 is the improvement made as the
 415 system was optimized.

416 The optimized catalyst mass flowrate is 341.5 kg/s which is a 12.15% increase on the 300
 417 kg/s base case condition. This would mean additional cost of feedstock to achieve 4.51 %
 418 increase in gasoline yield. This is consistent with the riser hydrodynamics where increase in
 419 mass flowrate of catalyst can result in increase in the reaction temperature. This is the case
 420 where it results in 1.19% increase in the temperature of the gas phase which in turn causes the
 421 increase in the yield of gases and gasoline. This optimization case shows that at optimized
 422 catalyst mass flowrate of 341.5 kg/s corresponding to catalyst-to-oil ratio (C/O) of 6.93. The
 423 gasoline throughput increases by 4.51%. The percentage increase may be considered
 424 appreciable because any small improvement in the optimal operation of the riser may lead to

425 large economic benefits ³⁻⁴. The riser output gas phase temperature in case 1 is 799.9 K,
 426 which is 2.9 °C lower than 802.8 K ¹⁰ in the literature. This shows reduced energy needed to
 427 achieve the case 1 optimum gasoline yield. Although, there increase in the feedstock mass
 428 flowrate to achieve the 4.51 % increase in gasoline throughput, there is a decrease of 2.9 °C
 429 gas phase temperature at the riser exit which reduces energy consumption in the process.

430

431 **Table 3:** Riser output for base case and optimized case 1

Riser Mass Fraction (kg-lump/kg-feed)	Base Case	Case 1	% Increase
Gas oil	0.296	0.249	6.26
Gasoline	0.529	0.554	4.51
Gases	0.136	0.157	13.38
Coke	0.039	0.040	2.50
Mass flowrate of gas oil (kg/s)	49.3	49.3	0.00
Mass flowrate of catalyst (kg/s)	300.0	341.5	12.15
Temperature of gas phase (K)	790.4	799.9	1.19
Temperature of catalyst phase (K)	791.5	800.9	1.17

432

433

434 Figure 8 shows weight fraction profiles of the four lumps; gas oil as feed while gasoline,
 435 gases and coke as products at both base case conditions and optimized conditions for case 2.
 436 The optimisation case 2 has its decision variable changed from the mass flow rate of catalyst
 437 in case 1 to mass flow rate of gas oil. The gas oil mass flow rate was set to be optimized
 438 between 20 kg/s to 100 kg/s, while the catalyst mass flow rate, gas-oil and catalyst
 439 temperature were set fixed at 300 kg/s, 535 K and 933 K respectively.

440

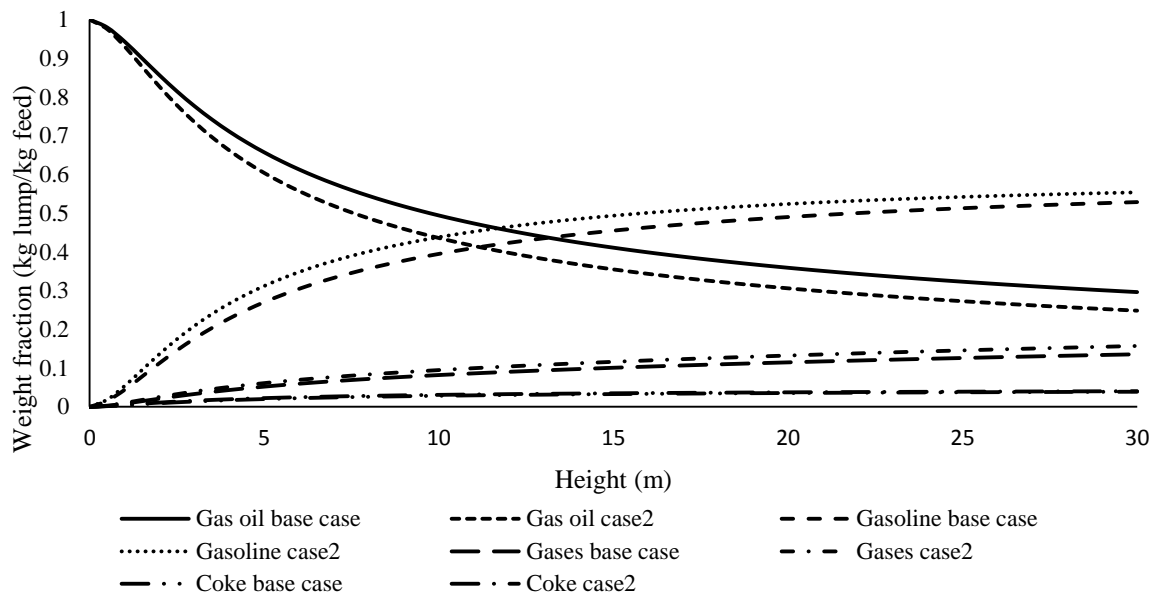


Figure 8: Four lump profile base and optimized cases 2

441

442 The unconverted gas oil in the base case condition is 0.296 kg-lump/kg-feed which is about
 443 70.40% conversion while the unconverted for the optimized case 2 is 0.248 kg-lump/kg-feed,
 444 which gives 6.38% increased conversion corresponding to 75.20% conversion of gas oil and
 445 results in 4.51%, 13.38% and 2.50% increase in gasoline, gases and coke respectively. Table
 446 4 shows the exit mass fractions and operating conditions for the base case and optimized case
 447 2. The percentage increase shown in Tables 4 is the improvement made when the system was
 448 optimized.

449

450 Table 4: Riser output for base case and optimized case 2

Riser Mass Fraction (kg-lump/kg-feed)	Base Case	Case 2	% Increase
Gas oil	0.296	0.248	6.38
Gasoline	0.529	0.554	4.51
Gases	0.136	0.157	13.38
Coke	0.039	0.040	2.50
Mass flowrate of gas oil (kg/s)	49.3	43.2	-14.12
Mass flowrate of catalyst (kg/s)	300.0	300.0	0.00
Temperature of gas phase (K)	790.4	800.0	1.20
Temperature of catalyst phase (K)	791.5	801.0	1.19

451

452 From Table 4, there is approximately 1.2% increase in both catalyst and gas phase
 453 temperatures, this means increase in the rate of cracking reaction because of the temperature

454 dependency of the rate of reaction leading to the increased conversion of gas oil by 6.38%,
455 increased yield of gasoline by 4.51%. More gases yield of 13.38 was accompanied including
456 2.5% increased coke deactivation. This is in spite of the decrease in the mass flowrate of gas
457 oil, however, the decrease in mass flow rate of gas oil means increased C/O ratio since the
458 mass flow rate of catalyst was held constant. This is consistent with operational principle of
459 increasing the C/O ratio to the riser to increase gasoline yield in the riser.

460 Although, the gas oil conversion in case 2 (75.20%) is slightly higher than in case 1
461 (75.10%), it gave no increase in the yield of gasoline, gases and coke. Although optimization
462 cases 1 and 2 gave similar results for all fractions, there was a slight increase (1.2%) in the
463 exit temperature of the gas phase from 790.9 K in case 1 to 800.0 K in case 2.

464 The optimized gas oil mass flowrate is 43.2 kg/s which is a 14.12% decrease on the 49.3 kg/s
465 base case condition. This corresponds to a 14.12% cut on the cost of feedstock which still
466 achieved the same 4.51% increase in the yield of gasoline. In case 2, a higher conversion is
467 obtained as gas oil mass flowrate is used compared with when the catalyst mass flow rate was
468 used in case 1. The riser output temperature in case 2 is 800.0 K, which is 2.8 K lower than
469 the value obtained by Han et al.¹⁰ (802.8 K). This shows that reduced energy needed to
470 achieve the case 2 optimum gasoline yield. This optimization case shows that at optimized
471 gas oil flowrate of 43.2 kg/s corresponding to catalyst-to-oil ratio (C/O) of 6.94, gasoline is
472 maximized by 4.51%. Again, a little improvement in the optimal operation of the riser may
473 lead to large economic benefits³⁻⁴.

474 Figure 9 shows the profiles of the four lumps; gas oil as feed while gasoline, gases and coke
475 as products at both base case conditions and optimized conditions for case 3.

476

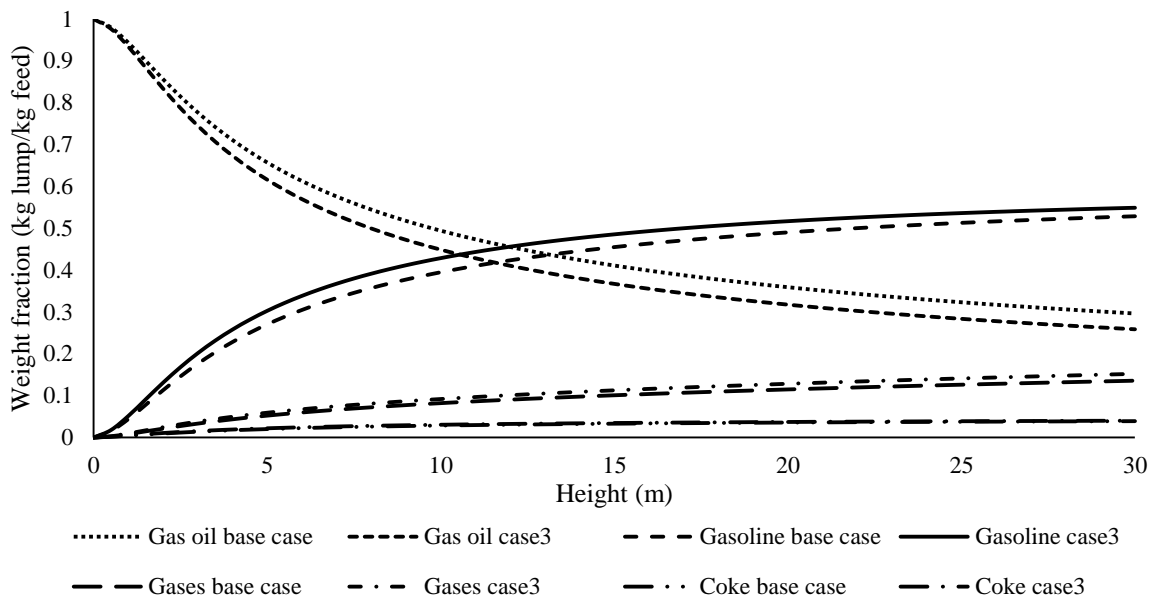


Figure 9: Four lump profile base and optimized cases 3

477

478 The optimisation case 3 used two decision variables, unlike cases 1 and 2. These were gas oil
 479 mass flowrate and catalyst mass flowrate. The gas oil mass flowrate was set to be optimized
 480 between 20 kg/s to 100 kg/s as in case 1, while the catalyst mass flow rate was set to be
 481 optimized between 100 kg/s to 500 kg/s as in case 2, whilst gas-oil and catalyst temperatures
 482 were fixed at 535 K and 933 K respectively.

483 Table 5 shows the exit mass fractions and operating conditions for the base case 3 and
 484 optimized case 3 along with percentage increases as the system was optimized.

485 Table 5: Riser output for base case and optimized case 3

Riser Mass Fraction (kg-lump/kg-feed)	Base Case	Case 3	% Increase
Gas oil	0.296	0.259	4.99
Gasoline	0.529	0.549	3.64
Gases	0.136	0.152	10.53
Coke	0.039	0.040	2.5
Mass flowrate of gas oil (kg/s)	49.3	44.8	-10.04
Mass flowrate of catalyst (kg/s)	300.0	310.8	3.47
Temperature of gas phase (K)	790.4	797.8	0.93
Temperature of catalyst phase (K)	791.5	801.0	1.19

486

487 The unconverted gas oil in the base case condition is 0.296 kg-lump/kg-feed which is about
 488 70.40% conversion while the unconverted for the optimized case 3 is 0.259 kg-lump/kg-feed
 489 (74.10%), which gives a difference of 4.99% increased conversion of gas oil and resulted in
 490 3.64%, 10.53% and 2.50% increase in gasoline, gases and coke respectively. Gas oil
 491 conversion in case 3 is 74.10% and it is slightly lower than in cases 1 (75.10%) and 2
 492 (75.20%).

493 The optimized gas oil mass flowrate is 44.8 kg/s which is a 10.04% decrease on the 49.3 kg/s
 494 base case condition, which means a 10.04% cut on the cost of feedstock into the riser. Also,
 495 the optimized catalyst mass flowrate is 310.8 kg/s which is a 3.47% increase on the 300 kg/s
 496 base case condition, which means an additional 3.47% cost of catalyst into the riser. This
 497 combination of the two decision variables; catalyst mass flowrate and gas oil mass flowrate is
 498 not the best use of operational decision because it produced the lower percentage increase of
 499 the yields of gasoline. The yield of gasoline is lower than cases 1 and 2 by 19.29%. Even
 500 though the yield of gases is lower in case 3 which is good for plant operation, the yield of
 501 gasoline was not favored due to lower conversion of gas oil compared with cases 1 and 2.

502 The riser output temperature of the gas phase in case 3 is 797.8 K, which is 5.0 °C lower than
 503 that quoted by Han et al.¹⁰ (802.8 K). This also shows a reduced energy needed to achieve the
 504 case 3 optimum gasoline yield. This optimization case shows that at optimized gas oil
 505 flowrate of 44.8 kg/s and catalyst mass flowrate 310.8 kg/s, which corresponds to a catalyst-
 506 to-oil ratio (C/O) of 6.94, gasoline is maximized by 3.64%.

507 Table 6 shows the yields of gasoline for all three optimization cases with their corresponding
 508 percentage increases.

509

510 Table 6: The yield of gasoline for cases 1, 2 and 3.

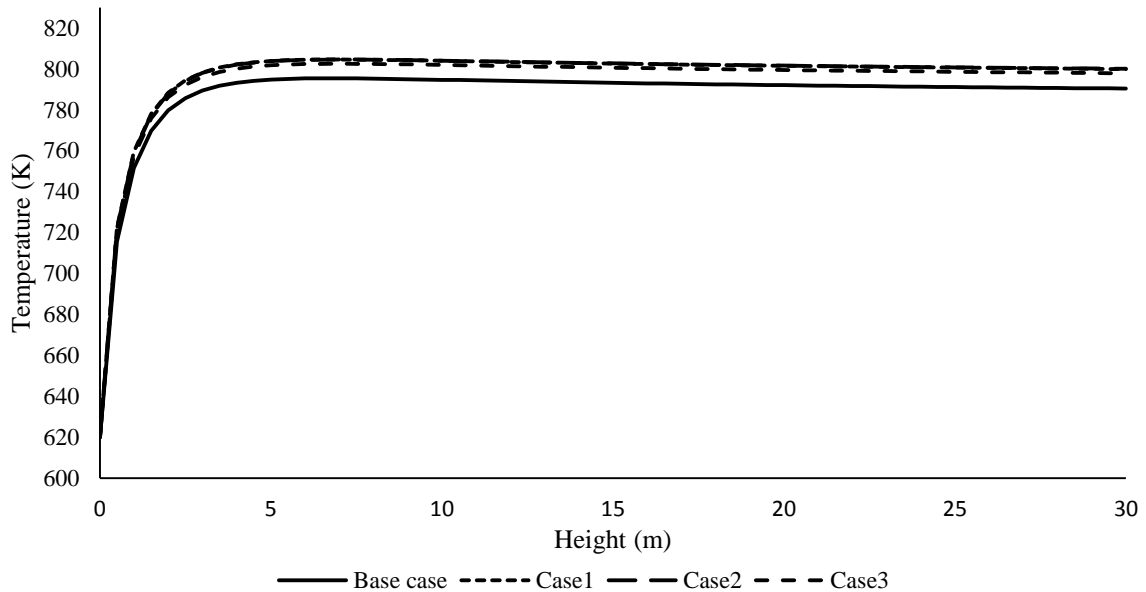
Riser Mass Fraction (kg-lump/kg-feed)	Base Case	Optimized Case	% Increase
Gasoline (Case 1)	0.529	0.554	4.51
Gasoline (Case 2)	0.529	0.554	4.51
Gasoline (Case 3)	0.529	0.549	3.64

511

512 In all the three cases, the yield of gasoline was increased by the optimization. Optimization
 513 case 2 gives the best result because it results in a 14.12% decrease in mass flowrate of feed,
 514 which means reducing the cost of feed and achieving a 4.51% improvement on the yield of
 515 gasoline. Though, case 1 also achieved a 4.51% increase in gasoline throughput, it has

516 12.15% increase in catalyst mass flowrate, which results in increased operating costs. Case 3
 517 shows a decrease of 10.04% in mass flowrate of feed but also has 3.47% increase in mass
 518 flowrate of catalyst, an additional cost as well with lower gasoline yield compared with case
 519 2.

520 Figure 10 shows exit temperature profiles of the gas phase for the base case condition which
 521 is 790.4 K, and the optimized cases 1, 2 and 3 with temperatures 799.9 K, 800.0 K and 800.0
 522 K respectively.



523 Figure 10: Gas phase temperature (base and optimized cases)

524 The gas phase temperature increases by an average of 10 K due to the slight increase in
 525 catalyst mass flowrate. However, the exit temperatures are consistent with the optimum value
 526 obtained in the literature ¹⁰.

527 The profiles in Figure 11 are exit temperatures of the catalyst phase for the base case
 528 condition (791.5 K) and cases 1, 2 and 3 with temperatures of 800.9 K, 801.0 K and 801.0 K
 529 respectively. Here, the catalyst gas phase temperature increases by an average of 10 K which
 530 is also due to the slight increase in the catalyst mass flowrate. Also, the exit temperatures are
 531 consistent with the optimum value obtained in the literature ¹⁰.

532

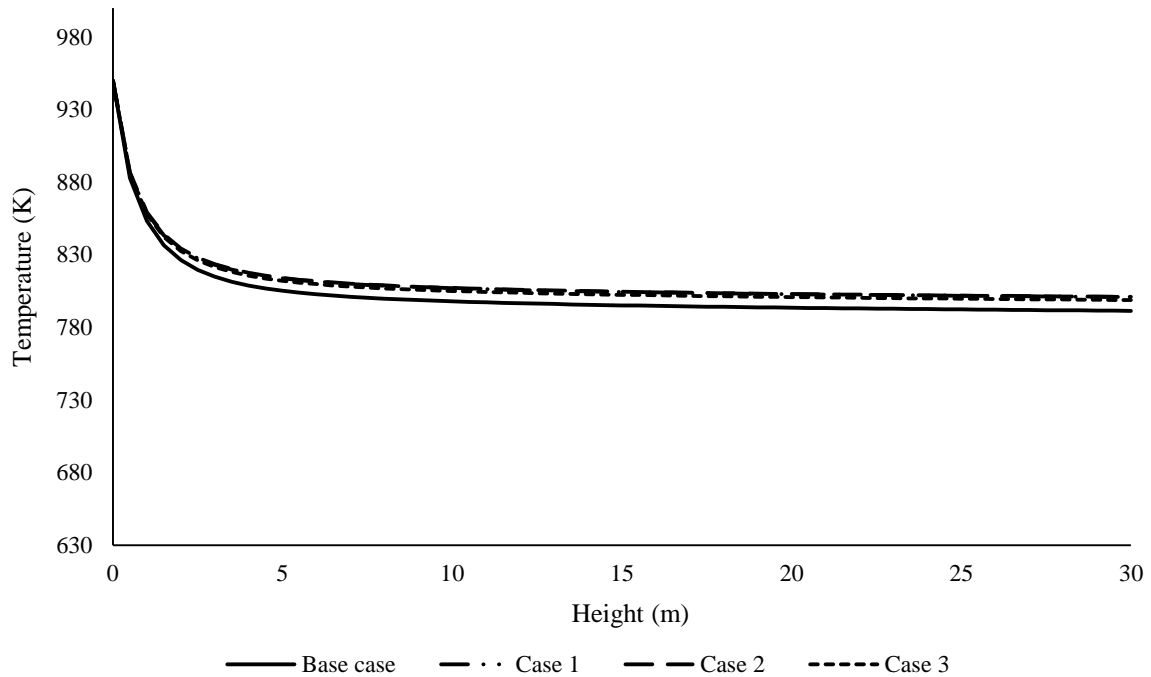


Figure 11: Catalyst phase temperature (base and optimized cases)

533

534 The pressures in the riser for base case condition and optimized cases 1, 2 and case 3 are
 535 presented in Figure 12. The base case pressure drop in the riser is 54.84 kPa, and for the
 536 optimized cases 1, 2 and 3 they are 54.02 kPa, 47.17 kPa and 49.08 kPa respectively. This
 537 shows a range of difference between the base case and optimized cases from 0.819 to 7.67
 538 kPa. Although, the qualitative profiles of the pressure drops in this simulation are similar to
 539 the ones obtained in the literature ⁹⁻¹⁰, the quantitative values differ (54.84 kPa in this work
 540 and 16 kPa by Han and Chung ⁹). As stated earlier, this may be because the vaporization
 541 section which considers the vapour pressure of the feed, taken into account by Han and
 542 Chung,⁹ was not considered in this work.

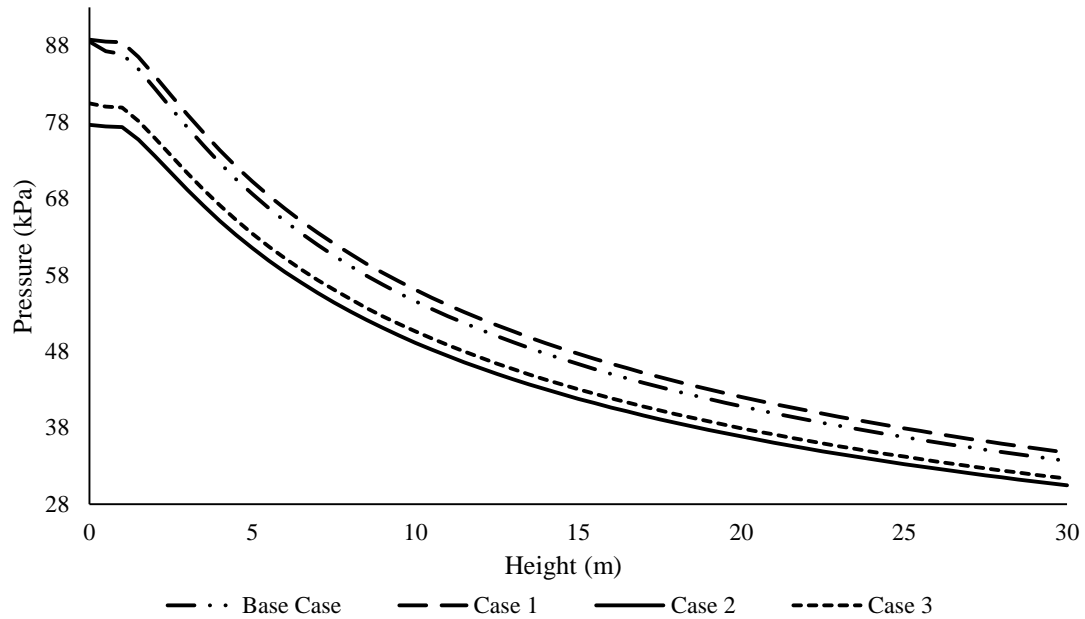


Figure 12: Pressure profiles for base and optimized cases

543

544 Figure 13 shows the catalyst phase velocity profiles which include the base case exit velocity
 545 (33.38 m/s) and exit velocities of the optimized cases 1, 2 and 3: 32.74 m/s, 32.74 m/s and
 546 32.88 m/s respectively. There is a difference between the velocities of the base case and
 547 optimized cases and the average decrease is in the range 0.50 to 0.64 m/s. The decrease in the
 548 optimal velocity may be attributed to the decrease in the pressure drop in the system.

549

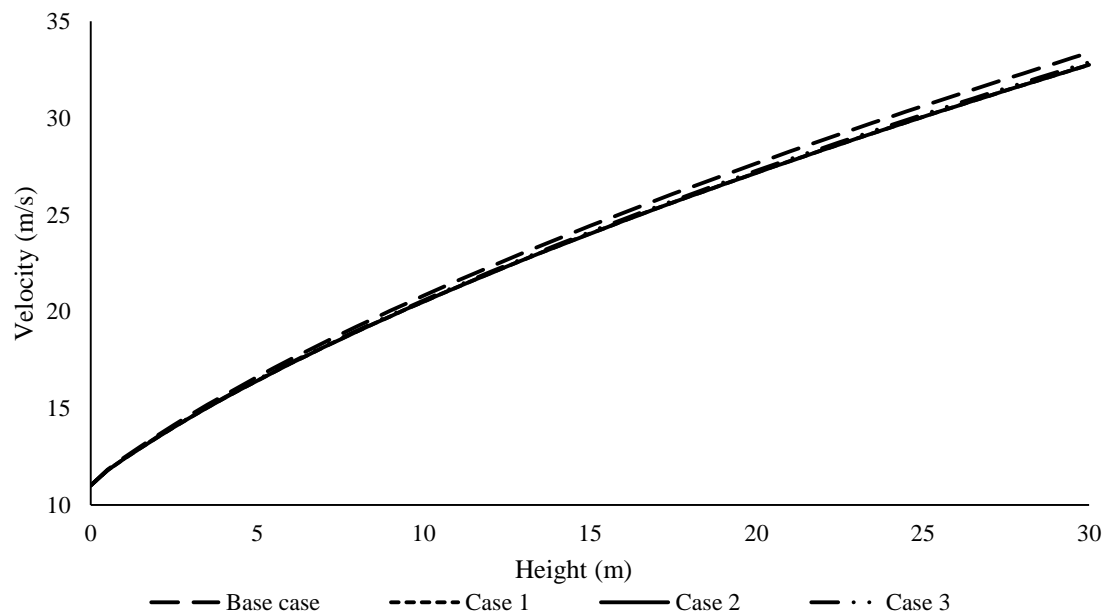


Figure 13: Catalyst velocity (base and optimized cases)

550

551

552 Figure 14 shows the gas phase velocity profiles which include the base case exit velocity
 553 (33.04 m/s) and exit velocities of the optimized cases 1, 2 and 3: 32.44 m/s, 32.43 m/s and
 554 32.56 m/s. An average difference between the velocities of the base case and optimized cases
 555 shows an increase in the range of 0.49 to 0.62 m/s. As before, the changes in the optimized
 556 gas phase velocities may be attributed to the corresponding changes in their pressure drop in
 557 the system.

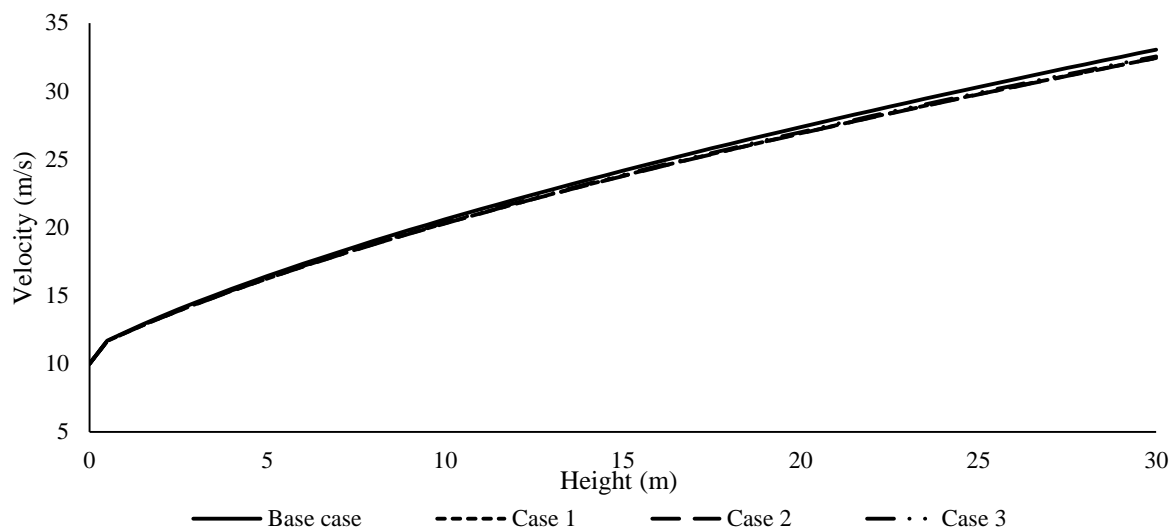


Figure 14: Gas phase velocity (base and optimized cases)

558

559 The riser exit temperatures of the gas phase in this work for the optimized cases 1, 2 and 3 are
 560 799.9 K, 800.0 K and 800.0 K respectively i.e. an average of 800 K. For the optimized cases
 561 in Han et al.¹⁰, the riser exit temperatures of the gas phase for both partial and complete
 562 combustion are from 801.6 K to 809.4 K i.e. an average of 805 K. Comparing the results, the
 563 riser exit temperature of the gas phase for this work is less by an average of 5 °C, which
 564 would result in a substantial reduction in energy consumption for the percentage increase in
 565 gasoline yield achieved in this work. The objective of the work of Han et al.¹⁰ was based on
 566 economic optimization and therefore the optimum yield of the gasoline was not presented as
 567 a separate lump. Hence, comparison with the maximized gasoline yield obtained in this work
 568 is difficult. However, the maximized gasoline yield of gasoline in this work (0.554 kg feed/kg
 569 lump) is 4.5% increase on the base case condition (0.529 kg feed/kg lump) and 7.6% increase
 570 on the gasoline yield of Han and Chung.⁸

571

572

573

574 **Conclusions**

575 In this work, optimization of the FCC has been carried out using a detailed process model to
576 maximize the conversion of gas oil to gasoline. A 4-lump kinetic model is assumed where gas
577 oil not only converts to gasoline but to two other undesired lumps; coke and gases. A steady
578 state optimization was carried out on a FCC riser and the following were found:

579 An optimal value of catalyst mass flowrate (341.5 kg/s) gave a maximized value for gasoline
580 yield as 0.554 kg-gasoline/kg-gas oil corresponding to 4.51% increase.

581 An optimal value of gas oil mass flowrate (43.2 kg/s) gave a maximized value for gasoline
582 yield as 0.554 kg-gasoline/kg-gas oil corresponding to 4.51% increase.

583 Concurrently using the optimal values of mass flowrates of catalyst (310.8 kg/s) and gas oil
584 (44.8 kg/s) in case 3 gives a lower gasoline yield 0.549 kg-gasoline/kg-gas oil. However, a
585 10.04% decrease in mass flowrate of gas oil was achieved with 8.68% reduction on the
586 optimum mass flowrate of catalyst in case 1. This shows that a good knowledge of the
587 operation of the riser can reduce cost, because the lost revenue from poorer yield could more
588 than offset any savings in operating costs²⁹ ,.

589 Following the increase in velocities of both the gas oil and catalyst phases from a range of
590 0.486 m/s to 0.637 m/s, and considering that the resident time of the riser is in the range of 1
591 to 2 s, the velocity variation is large enough to affect the riser hydrodynamics and
592 consequently the yield of gasoline. Similarly, the pressure drop variation is from 0.818 kPa to
593 7.67 kPa, significant enough to change the hydrodynamics of the riser.

594

595 **Notation**

A	Surface area, m ²
A_{ptc}	Effective interface heat transfer area per unit volume, m ² /m ³
C	Mole concentration, kg mole/m ³
C_{pg}	Gas heat capacity, kJ/kg K
C_{ps}	Solid heat capacity, kJ/kg K
D	Diameter, m
d_c	Catalyst average diameter, m
E	Activation energy, kJ/kg mole
F	Mass flow rate, kg/s
Gc	Stress modulus, kg/m s ²
H	Specific enthalpy, kJ/kg

ΔH	Heat of reaction kJ/kg
h	Enthalpy of reaction kJ/kg
h_p	Interface heat transfer coefficient between the catalyst and gas phases
h_T	Interface heat transfer coefficient, kJ/m ² s K
k_{i0}	Frequency factor in the Arrhenius expression, 1/s
K_i	Rate coefficient of the four-lump cracking reaction, 1/s
K_g	Thermal conductivity of hydrocarbons
L	Length, m
M_w	Molecular weight
P	Pressure , kPa
Q_{react}	Rate of heat generation or heat removal by reaction, kJ/s
R	Ideal gas constant, 8.3143 kPa m ³ /-kg mole K or kJ/kg mole K
RAN	Aromatics-to-naphthenes ratio in liquid feedstock
S_c	Average sphericity of catalyst particles
S_g	Total mass interchange rate between the emulsion and bubble phases, 1/s
T	Temperature, K
u	superficial velocity, m/s
V	Volume, m ³
y	Weight fraction
Z_g	Gas compressibility factor

Greek

Ω	Cross-sectional area
ρ	Density, kg/m ³
\emptyset	Catalyst deactivation function
ε	Voidage
α	Catalyst deactivation coefficient
α_c^*	exponent for representing α
μ_g	viscosity

Subscript

cc	Coke on catalyst
ck	Coke
g	Acceleration m/s ²
gl	Gasoline

go	Gas oil
gs	Gases
MABP	Molal average boiling temperature, K
MeABP	Mean average boiling temperature, K
pc	pseudo-critical
pr	pseudo-reduced
Rs	Riser

596

597 **Acknowledgement:**

598 Petroleum Technology Development Fund, Nigeria, financially sponsored the study.

599

600 **Appendix A**

601 Equations A.1 – A.24 are correlations of physical and transport parameters adopted from the
602 literature⁸⁻⁹.

603 Heat capacity of gas, C_{pg} , is

$$604 C_{pg} = \beta_1 + \beta_2 T_g + \beta_3 T_g^2 \quad (A.1)$$

605 Where β_1 , β_2 , β_3 and β_4 catalyst decay constant given as

$$606 \beta_1 = -1.492343 + 0.124432K_f + \beta_4 \left(1.23519 - \frac{1.04025}{S_g} \right)$$

$$607 (A.2)\beta_2 = (-7.53624 \times 10^{-4}) \left[2.9247 - (1.5524 - 0.05543K_f)K_f + \beta_4 \left(6.0283 - \right. \right.$$

$$608 \quad (A.3)$$

$$610 \quad (A.3)$$

$$611 \beta_3 = (1.356523 \times 10^{-6})(1.6946 + 0.0884\beta_4) \quad (A.4)$$

$$612 \beta_4 = \left[\left(\frac{12.8}{K_f} - 1 \right) \left(1 - \frac{10}{K_f} \right) (S_g - 0.885)(S_g - 0.7)(10^4) \right]^2 \text{ For } 10 < K_f < 12.8 \quad (A.5)$$

613 Else $\beta_4 = 0$ for all other cases

614 K_f is the Watson characterization factor written as

$$615 K_f = \frac{(1.8T_{MeABP})^{\frac{1}{3}}}{S_g} \quad (A.6)$$

616 Where M_{wg} is the molecular weight of the gas and can be calculated using

617 $M_{wg} =$
618 $42.965[\exp(2.097 \times 10^{-4}T_{MeABP} - 7.787S_g + 2.085 \times$
619 $10^{-3}T_{MeABP}S_g)] (T_{MeABP}^{1.26007} S_g^{4.98308})$ (A.7)

620 $T_{MeABP} = T_{VABP} - 0.5556\exp[-0.9440 - 0.0087(1.8T_{VABP} - 491.67)^{0.6667} +$
621 $2.9972(SI)^{0.3333}$ (A.8)

622 Where T_{VABP} , the volume average boiling temperature and (SI) is slope given as

623 $(SI) = 0.0125(T_{90ASTM} - T_{10ASTM})$ (A.9)

624 In order to calculate the ASTM D86 distillation temperatures, a_i , b_i and T_{iTBP}
625 values were used where a_i and b_i are distillation coefficients and T_{iTBP} is the true boiling
626 point distillation temperature as shown in Table A.2.

627 $T_{VABP} = 0.2(T_{10ASTM} + T_{30ASTM} + T_{50ASTM} + T_{70ASTM} + T_{90ASTM})$ (A.10)

628 The ASTM D86 distillation temperatures are calculated using

629 $T_{10ASTM} = a_{10}^{-\frac{1}{b_{10}}}(T_{10TBP})^{\frac{1}{b_{10}}}$ (A.11)

630 $T_{30ASTM} = a_{30}^{-\frac{1}{b_{30}}}(T_{30TBP})^{\frac{1}{b_{30}}}$ (A.12)

631 $T_{50ASTM} = a_{50}^{-\frac{1}{b_{50}}}(T_{50TBP})^{\frac{1}{b_{50}}}$ (A.13)

632 $T_{70ASTM} = a_{70}^{-\frac{1}{b_{70}}}(T_{70TBP})^{\frac{1}{b_{70}}}$ (A.14)

633 $T_{90ASTM} = a_{90}^{-\frac{1}{b_{90}}}(T_{90TBP})^{\frac{1}{b_{90}}}$ (A.15)

634 Interface heat transfer coefficient between the catalyst and gas phases, h_p ,

635 $h_p = 0.03 \frac{K_g}{d_c^{\frac{2}{3}}} \left[\frac{|(v_g - v_c)| \rho_g \epsilon_g}{\mu_g} \right]^{\frac{1}{3}}$ (A.16)

636 Thermal conductivity of hydrocarbons

637 $K_g = 1 \times 10^{-6}(1.9469 - 0.374M_{wm} + 1.4815 \times 10^{-3}M_{wm}^2 + 0.1028T_g)$ (A.17)

638 M_{WM} is the mean molecular weight of the combined catalyst and gas

639 $M_{WM} = \frac{1}{\left(\frac{y_{go}}{M_{wgo}} + \frac{y_{gl}}{M_{wgl}} + \frac{y_{gs}}{M_{wgs}} + \frac{y_{ck}}{M_{wck}} \right)}$ (A.18)

640 $M_{wgo} = M_{wg}$ (A.19)

641 $M_{wgs} = 0.002M_{wH_2} + 0.057M_{wC_1} + 0.078M_{wC_2} + 0.297M_{wC_3} + 0.566M_{wC_4}$ (A.20)

642 The viscosity of the gas

$$643 \quad \mu_g = 3.515 \times 10^{-8} \mu_{pr} \sqrt{\frac{M_{WM} P_{pc}^{\frac{2}{3}}}{T_{pc}^{\frac{1}{6}}}} \quad (A.21)$$

$$644 \quad \mu_{pr} = 0.435 \exp[(1.3316 - T_{pr}^{0.6921}) P_{pr}] T_{pr} + 0.0155 \quad (A.22)$$

$$645 \quad T_{pc} = 17.1419 [\exp(-9.3145 \times 10^{-4} T_{MeABP} - 0.5444 S_g + 6.4791 \times 10^{-4} T_{MeABP} S_g)] \\ \times T_{MeAB}^{-0.4844} S_g^{4.0846} \quad (A.23)$$

$$646 \quad P_{pc} = 4.6352 \times 10^6 [\exp(-8.505 \times 10^{-3} T_{MeABP} - 4.8014 S_g + 5.749 \times 10^{-3} T_{MeABP} S_g)] \\ \times T_{MeAB}^{-0.4844} S_g^{4.0846} \quad (A.24)$$

648 Catalyst-gas friction coefficient C_f ¹⁸

$$649 \quad C_f = 150 \frac{\varepsilon_c^2 \mu_g \rho_c}{(\varepsilon_g d_c S_c)^2 (\rho_c - \rho_g)} + 1.75 \frac{\rho_g \rho_c |(v_g - v_c)| \varepsilon_c}{\varepsilon_g d_c S_c (\rho_c - \rho_g)} \quad \text{for } \varepsilon_g < 0.8 \quad (A.25)$$

$$650 \quad C_f = \frac{3}{4} C_d \frac{|(v_g - v_c)| \rho_c \rho_g \varepsilon_c}{d_c S_c (\rho_c - \rho_g)} \varepsilon_g^{-2.65} \quad \text{for } \varepsilon_g > 0.8 \quad (A.26)$$

651 Drag coefficient defined as

$$652 \quad C_d = \frac{24}{Re_c} (1 + 0.15 Re_c^{0.687}) \quad \text{for } Re_c < 1000 \quad (A.27)$$

$$653 \quad C_d = 0.44 \quad \text{for } Re_c > 1000 \quad (A.28)$$

654 The Reynolds number for the catalyst and gas are written as

$$655 \quad Re_c = \frac{|(v_g - v_c)| d_c F_g}{\mu_g v_g \Omega} \quad (A.29)$$

$$656 \quad Re_g = \frac{v_g D \rho_g \varepsilon_g}{\mu_g} \quad (A.30)$$

657 Finally, the friction coefficients of the catalyst and gas can be calculated using

$$658 \quad f_{rc} = \frac{0.05}{v_c} \quad (A.31)$$

$$659 \quad f_{rg} = \frac{16}{Re_g} \quad \text{for } Re_g < 2100 \quad (A.32)$$

$$660 \quad f_{rg} = 0.0791 Re_g^{-0.25} \quad \text{for } 2.1 \times 10^3 < Re_g < 10^5 \quad (A.33)$$

$$661 \quad f_{rg} = 0.0008 + 0.0552 Re_g^{-0.237} \quad \text{for } 10^5 < Re_g < 10^8 \quad (A.34)$$

662 The molecular weights of hydrogen, M_{wH_2} , methane, M_{wC_1} , ethane, M_{wC_2} , propane, M_{wC_3} ,

663 and butane, M_{wC_4} are specified in Table A.3.

664

665 Table A.1: Total number of model equations for degree of freedom analysis

Nos	Equation	Eqn. No.
1	$\frac{dT_c}{dx} = \frac{\Omega h_p A_p}{F_c C_{pc}} (T_g - T_c)$	1

2	$\frac{dT_g}{dx} = \frac{\Omega}{F_g C_{pg}} [h_p A_p (T_c - T_g) + \rho_c \varepsilon_c Q_{react}]$	2
3	$\frac{dy_{go}}{dx} = \frac{\rho_c \varepsilon_c \Omega \phi_c}{F_g} R_{go}$	3
4	$\frac{dy_{gl}}{dx} = \frac{\rho_c \varepsilon_c \Omega \phi_c}{F_g} R_{gl}$	4
5	$\frac{dy_{gs}}{dx} = \frac{\rho_c \varepsilon_c \Omega \phi_c}{F_g} R_{gs}$	5
6	$\frac{dy_{ck}}{dx} = \frac{\rho_c \varepsilon_c \Omega}{F_g} R_{ck}$	6
7	$\frac{dv_c}{dx} = - \left(G_c \frac{\Omega}{F_c} \frac{d\varepsilon_c}{dx} - \frac{C_f (v_g - v_c) \Omega}{F_c} + \frac{2f_{rc} v_c}{D} + \frac{g}{v_c} \right)$	29
8	$\frac{dv_g}{dx} = - \left(\frac{\Omega}{F_g} \frac{dP}{dx} - \frac{C_f (v_c - v_g)}{F_g} + \frac{2f_{rg} v_g}{D} + \frac{g}{v_g} \right)$	30
9	$R_{go} = -(K_1 + K_2 + K_3) y_{go}^2$	7
10	$R_{gl} = (K_1 y_{go}^2 - K_4 y_{gl} - K_5 y_{gl})$	8
11	$R_{gs} = (K_2 y_{go}^2 - K_4 y_{gl})$	9
12	$R_{ck} = (K_3 y_{go}^2 - K_5 y_{gl})$	10
13	$K_1 = k_{10} \exp\left(\frac{-E_1}{RT_g}\right)$	11
14	$K_2 = k_{20} \exp\left(\frac{-E_2}{RT_g}\right)$	12
15	$K_3 = k_{30} \exp\left(\frac{-E_3}{RT_g}\right)$	13
16	$K_4 = k_{40} \exp\left(\frac{-E_4}{RT_g}\right)$	14
17	$k_5 = K_{50} \exp\left(\frac{-E_5}{RT_g}\right)$	15
18	$Q_{react} = -(\Delta H_1 K_1 y_{go}^2 + \Delta H_2 K_2 y_{go}^2 + \Delta H_3 K_3 y_{go}^2 + \Delta H_4 K_4 y_{gl} + \Delta H_5 K_5 y_{gl}) \phi_c$	16
19	$\varepsilon_g = 1 - \varepsilon_c$	17
20	$\varepsilon_c = \frac{F_c}{v_c \rho_c \Omega}$	18

21	$\Omega = \frac{\pi D^2}{4}$	19
22	$A_{ptc} = \frac{6}{0.72d_c} * (1 - \varepsilon_g)$	20
23	$\phi_c = \exp(-\alpha_c C_{ck})$	21
24	$\alpha_c = \alpha_{c0} \exp\left(\frac{-E_c}{RT_g}\right) (R_{AN})^{\alpha_{c*}}$	22
25	$C_{ck} = C_{ckCL1} + \frac{F_g y_{ck}}{F_c}$	23
26	$\rho_g = \frac{F_g}{\varepsilon_g v_g \Omega}$	24
27	$P = \rho_g \frac{RT_g}{M_{wg}}$	25
28	$T_{pr} = \frac{T_g}{T_{pc}}$	27
29	$P_{pr} = \frac{P}{P_{pc}}$	28
30	$G_c = 10^{(-8.76\varepsilon_g R_S + 5.43)}$	31
31	$C_{pg} = \beta_1 + \beta_2 T_g + \beta_3 T_g^2$	A.1
32	$\beta_1 = -1.492343 + 0.124432K_f + \beta_4 \left(1.23519 - \frac{1.04025}{S_g}\right)$	A.2
33	$\beta_2 = (-7.53624 \times 10^{-4}) \left[2.9247 - (1.5524 - 0.05543K_f)K_f + \beta_4 \left(6.0283 - \frac{5.0694}{S_g}\right)\right]$	A.3
34	$\beta_3 = (1.356523 \times 10^{-6})(1.6946 + 0.0884\beta_4)$	A.4
35	$\beta_4 = \left[\left(\frac{12.8}{K_f} - 1\right)\left(1 - \frac{10}{K_f}\right)(S_g - 0.885)(S_g - 0.7)(10^4)\right]^2$	A.5
36	$K_f = \frac{(1.8T_{MeABP})^{\frac{1}{3}}}{S_g}$	A.6
37	$M_{wg} = 42.965 \left[\exp(2.097 \times 10^{-4} T_{MeABP} - 7.787 S_g + 2.085 \times 10^{-3} T_{MeABP} S_g) \right] (T_{MeABP}^{1.26007} S_g^{4.98308})$	A.7
38	$T_{MeABP} = T_{VABP} - 0.5556 \exp[-0.9440 - 0.0087(1.8T_{VABP} - 491.67)^{0.6667} + 2.9972(SI)^{0.3333}]$	A.8
39	$(SI) = 0.0125(T_{90ASTM} - T_{10ASTM})$	A.9

$$40 \quad T_{VABP} = 0.2(T_{10ASTM} + T_{30ASTM} + T_{50ASTM} + T_{70ASTM} + T_{90ASTM}) \quad A.10$$

$$41 \quad T_{10ASTM} = a_{10} \frac{1}{b_{10}^{10}} (T_{10TBP})^{\frac{1}{b_{10}}} \quad A.11$$

$$42 \quad T_{30ASTM} = a_{30} \frac{1}{b_{30}^{30}} (T_{30TBP})^{\frac{1}{b_{30}}} \quad A.12$$

$$43 \quad T_{50ASTM} = a_{50} \frac{1}{b_{50}^{50}} (T_{50TBP})^{\frac{1}{b_{50}}} \quad A.13$$

$$44 \quad T_{70ASTM} = a_{70} \frac{1}{b_{70}^{70}} (T_{70TBP})^{\frac{1}{b_{70}}} \quad A.14$$

$$45 \quad T_{90ASTM} = a_{90} \frac{1}{b_{90}^{90}} (T_{90TBP})^{\frac{1}{b_{90}}} \quad A.15$$

$$46 \quad h_p = 0.03 \frac{K_g}{d_c^{\frac{2}{3}}} \left[\frac{|(v_g - v_c)| \rho_g \varepsilon_g}{\mu_g} \right]^{\frac{1}{3}} \quad A.16$$

$$47 \quad K_g = 1 \times 10^{-6} (1.9469 - 0.374M_{wm} + 1.4815 \times 10^{-3}M_{wm}^2 + 0.1028T_g) \quad A.17$$

$$48 \quad M_{WM} = \frac{1}{\left(\frac{y_{go}}{M_{wgo}} + \frac{y_{gl}}{M_{wgl}} + \frac{y_{gs}}{M_{wgs}} + \frac{y_{ck}}{M_{wck}} \right)} \quad A.18$$

$$49 \quad M_{wgs} = 0.002M_{wH_2} + 0.057M_{wC_1} + 0.078M_{wC_2} + 0.297M_{wC_3} + 0.566M_{wC_4} \quad A.20$$

$$50 \quad \mu_g = 3.515 \times 10^{-8} \mu_{pr} \frac{\sqrt{M_{WM} P_{pc}^{\frac{2}{3}}}}{T_{pc}^{\frac{1}{6}}} \quad A.21$$

$$51 \quad \mu_{pr} = 0.435 \exp[(1.3316 - T_{pr}^{0.6921})P_{pr}] T_{pr} + 0.0155 \quad A.22$$

$$52 \quad T_{pc} = 17.1419 \left[\exp(-9.3145 \times 10^{-4}T_{MeABP} - 0.5444S_g + 6.4791 \times 10^{-4}T_{MeABP}S_g) \right] \times T_{MeAB}^{-0.4844} S_g^{4.0846} \quad A.23$$

$$53 \quad P_{pc} = 4.6352 \times 10^6 \left[\exp(-8.505 \times 10^{-3}T_{MeABP} - 4.8014S_g + 5.749 \times 10^{-3}T_{MeABP}S_g) \right] \times T_{MeAB}^{-0.4844} S_g^{4.0846} \quad A.24$$

$$54 \quad C_f = 150 \frac{\varepsilon_c^2 \mu_g \rho_c}{(\varepsilon_g d_c S_c)^2 (\rho_c - \rho_g)} + 1.75 \frac{\rho_g \rho_c |(v_g - v_c)| \varepsilon_c}{\varepsilon_g d_c S_c (\rho_c - \rho_g)} \quad \text{for } \varepsilon_g < 0.8 \quad A.25$$

$$OR \quad C_f = \frac{3}{4} C_d \frac{|(v_g - v_c)| \rho_c \rho_g \varepsilon_c}{d_c S_c (\rho_c - \rho_g)} \varepsilon_g^{-2.65} \quad \text{for } \varepsilon_g > 0.8 \quad A.26$$

55	$C_d = \frac{24}{Re_c} (1 + 0.15 Re_c^{0.687})$	for $Re_c < 1000$	A.27
OR	$C_d = 0.44$	for $Re_c > 1000$	A.28
56	$Re_c = \frac{ (v_g - v_c) d_c F_g}{\mu_g v_g \Omega}$		A.29
57	$Re_g = \frac{v_g D \rho_g \varepsilon_g}{\mu_g}$		A.30
58	$f_{rc} = \frac{0.05}{v_c}$		A.31
59	$f_{rg} = \frac{16}{Re_g}$	for $Re_g < 2100$	A.32
OR	$f_{rg} = 0.0791 Re_g^{-0.25}$	for $2.1 \times 10^3 < Re_g < 10^5$	A.33
OR	$f_{rg} = 0.0008 + 0.0552 Re_g^{-0.237}$	for $10^5 < Re_g < 10^8$	A.34

666

667 Table A.2: Specifications of variables.

Variables	Total
$T_c(x), T_g(x), y_{go}(x), y_{gl}(x), y_{gs}(x), y_{ck}(x), v_c(x), v_g(x), R_{go}, R_{gl}, R_{gs}, R_{ck}, K_1, K_2,$ $K_3, K_4, K_5, Q_{react}, \emptyset_c, \alpha_c, A_{ptc}, \Omega, \varepsilon_c, \varepsilon_g, C_{ck}, \rho_g, P, T_{pr}, P_{pr}, G_c, f_{rc}, f_{rg}, M_{wg}, C_{pg}, \beta_1,$ $\beta_2, \beta_3, \beta_4, K_f, T_{MeABP}, S_l, T_{VABP}, T_{10ASTM}, T_{30ASTM}, T_{50ASTM}, T_{70ASTM}, T_{90ASTM}, h_p,$ $K_g, M_{WM}, \mu_g, T_{pc}, P_{pc}, C_f, C_d, Re_c, Re_g, C_{pc}, M_{wH_2}, M_{wC_1}, M_{wC_2}, M_{wC_3}, F_g, F_c,$ $M_{wC_4}, \rho_c, g, R, E_1, E_2, E_3, E_4, E_5, k_{10}, k_{20}, k_{30}, k_{40}, k_{50}, \Delta H_1, \Delta H_2, \Delta H_3, \Delta H_4, \Delta H_5,$ $d_c, \alpha_{c*}, R_{AN}, E_c, \alpha_{c0}, C_{ckCL1}, D, S_g, T_{10TBP}, T_{20TBP}, T_{30TBP}, T_{40TBP}, T_{50TBP},$ $b_{10}, b_{20}, b_{30}, b_{70}, b_{90}, a_{10}, a_{30}, a_{50}, a_{70}, a_{90}, \mu_{pr}, M_{wgo}, M_{wgl}, M_{wgs}, M_{wck}$ and $S_c.$	112
Differential variables at $x = 0,$	8
$\frac{dT_c}{dx}, \frac{dT_g}{dx}, \frac{dy_{go}}{dx}, \frac{dy_{gl}}{dx}, \frac{dy_{gs}}{dx}, \frac{dy_{ck}}{dx}, \frac{dv_c}{dx}$ and $\frac{dv_g}{dx}$	
Independent variable; x	1
Total	121

668

669 Table A.3 summarizes the variables and parameters to satisfy the degree of freedom. The
670 feed and catalyst characteristic and other parameters used in this simulation. Most of the
671 parameters were obtained from the industry and literature^{9, 30-31}.

672

673 Table A.3: Specifications of constant parameters and differential variables at $x = 0$.

Variable	Value
Riser Height, x (m)	30
$T_g(0)$ (Temperature of gas oil, K)	535
$T_c(0)$ (Temperature of gas catalyst, K)	933
$v_c(0)$ Velocity of catalyst (m/s)	12
$v_g(0)$ Velocity of gas oil (m/s)	10
D Riser Diameter (m)	1.1
F_c (Catalyst mass flowrate, kg/s)	300
F_g (Gas oil mass flowrate, kg/s)	49.3
$y_{go}(0)$ Mass fraction of gas oil	1.0
$y_{gl}(0)$ Mass fraction of gas oil	0.0
$y_{gs}(0)$ Mass fraction of gas oil	0.0
$y_{ck}(0)$ Mass fraction of gas oil	0.0
M_{wgo} Molecular weight gas oil (kg/k mol)	371
M_{wgl} Molecular weight gasoline (kg/k mol)	106.7
M_{wck} Molecular weight coke (kg/k mol)	14.4
d_c (Average particle diameter, m)	0.00007
S_c (Average sphericity of catalyst particles)	0.72
S_g (Specific gravity)	0.897
C_{ckCL1} (Coke on catalyst, kg coke/kg catalyst)	0.001
α_{c0} (pre-exponential factor of α_c)	1.1e-5
α_{c*} (Catalyst deactivation coefficient)	0.1177
C_{pc} (Heat capacity of catalyst, kJ/kg K)	1.15
ρ_c (Density of catalyst, kg/m ³)	1410
R_{AN} (Aromatics/Naphthenes in liquid feedstock)	2.1
T_{10TBP} TBP distilled 10 volume%, °C	554.3
T_{30TBP} , TBP distilled 30 volume %, °C	605.4
T_{50TBP} , TBP distilled 50 volume %, °C	647.0
T_{70TBP} TBP distilled 70 volume %, °C	688.2
T_{90TBP} TBP distilled 90 volume %, °C	744.8
a_{10} Distillation Coefficients 10 volume%	0.5277
a_{30} Distillation Coefficients 30 volume %	0.7429

a ₅₀ Distillation Coefficients 50 volume %	0.8920
a ₇₀ Distillation Coefficients 70 volume %	0.8705
a ₉₀ Distillation Coefficients 90 volume %	0.9490
b ₁₀ Distillation Coefficients 10 volume %	1.0900
b ₃₀ Distillation Coefficients 30 volume %	1.0425
b ₅₀ Distillation Coefficients 50 volume %	1.0176
b ₇₀ Distillation Coefficients 70 volume %	1.0226
b ₉₀ Distillation Coefficients 90 volume %	1.0110
k ₁₀ Frequency factor (s ⁻¹)	1457.50
k ₂₀ Frequency factor (s ⁻¹)	127.59
k ₃₀ Frequency factor (s ⁻¹)	1.98
k ₄₀ Frequency factor (s ⁻¹)	256.81
k ₅₀ Frequency factor (s ⁻¹)	6.29e-4
E ₁ Activation Energy (kJ/kg mol)	57,359
E ₂ Activation Energy (kJ/kg mol)	52,754
E ₃ Activation Energy (kJ/kg mol)	31,820
E ₄ Activation Energy (kJ/kg mol)	65,733
E ₅ Activation Energy (kJ/kg mol)	66,570
E _c Catalyst Activation Energy (kJ/kg mol)	49,000
ΔH ₁ Heat of reaction (kJ/kg)	195
ΔH ₂ Heat of reaction (kJ/kg)	670
ΔH ₃ Heat of reaction (kJ/kg)	745
ΔH ₄ Heat of reaction (kJ/kg)	530
ΔH ₅ Heat of reaction (kJ/kg)	690
M _{wH₂} Molecular weights of hydrogen (kg/k mol)	2
M _{wC₁} Molecular weights of methane (kg/k mol)	16
M _{wC₂} Molecular weights of ethane (kg/k mol)	30
M _{wC₃} Molecular weights of propane (kg/k mol)	44
M _{wC₄} Molecular weights of butane (kg/k mol)	58
g, acceleration due to gravity (m/s ²)	9.8
R, ideal gas constant (kPa m ³ /kg mole K)	8.3143

674

675

676

677

678

679 **REFERENCES:**

680 (1) Bollas, G. M.; Lappas, A. A.; Iatridis, D. K.; Vasalos, I. A., Five-lump kinetic model with
681 selective catalyst deactivation for the prediction of the product selectivity in the fluid
682 catalytic cracking process. *Catalysis Today* **2007**, *127* (1-4), 31-43.

683 (2) Almeida, N. E.; Secchi, A. R., Dynamic Optimization of a FCC Converter Unit:
684 Numerical Analysis. *Brazilian Journal of Chemical Engineering* **2011**, *28* (01), 117-136.

685 (3) Zanin, A. C.; Tvrzská de Gouvêa, M.; Odloak, D., Integrating real-time optimization into
686 the model predictive controller of the FCC system. *Control Engineering Practice* **2002**, *10*
687 (8), 819-831.

688 (4) Vieira, W. G.; Santos, V. M. L.; Carvalho, F. R.; Pereira, J. A. F. R.; Fileti, A. M. F.,
689 Identification and predictive control of a FCC unit using a MIMO neural model. *Chemical*
690 *Engineering and Processing: Process Intensification* **2005**, *44* (8), 855-868.

691 (5) Sankararao, B.; Gupta, S. K., Multi-objective optimization of an industrial fluidized-bed
692 catalytic cracking unit (FCCU) using two jumping gene adaptations of simulated annealing.
693 *Computers & Chemical Engineering* **2007**, *31* (11), 1496-1515.

694 (6) Bispo, V. D. S.; Silva, E. S. R. L.; Meleiro, L. A. C., Modeling, Optimization and Control
695 of a FCC Unit Using Neural Networks and Evolutionary Methods. *Engevista* **2014**, *16* (1), 70
696 - 90.

697 (7) Souza, J. A.; Vargas, J. V. C.; Ordonez, J. C.; Martignoni, W. P.; von Meien, O. F.,
698 Thermodynamic optimization of fluidized catalytic cracking (FCC) units. *International*
699 *Journal of Heat and Mass Transfer* **2011**, *54* (5-6), 1187-1197.

700 (8) Han, I.-S.; Chung, C.-B., Dynamic modeling and simulation of a fluidized catalytic
701 cracking process. Part I: Process modeling. *Chemical Engineering Science* **2001**, *56* (5),
702 1951-1971.

703 (9) Han, I.-S.; Chung, C.-B., Dynamic modeling and simulation of a fluidized catalytic
704 cracking process. Part II: Property estimation and simulation. *Chemical Engineering Science*
705 **2001**, *56* (5), 1973-1990.

706 (10) Han, I.-S.; Riggs, J. B.; Chung, C.-B., Modeling and optimization of a fluidized catalytic
707 cracking process under full and partial combustion modes. *Chemical Engineering &*
708 *Processing: Process Intensification* **2004**, *43* (8), 1063-1084.

709 (11) Theologos, K. N.; Markatos, N. C., Advanced modeling of fluid catalytic cracking riser-
710 type reactors. *AIChE Journal* **1993**, *39* (6), 1007-1017.

711 (12) Ali, H.; Rohani, S.; Corriou, J. P., Modelling and Control of a Riser Type Fluid Catalytic
712 Cracking (FCC) Unit. *Chemical Engineering Research and Design* **1997**, *75* (4), 401-412.

713 (13) Lee, L.-S.; Yu, S.-W.; Cheng, C.-T., Fluidized-bed Catalyst Cracking Regenerator
714 Modelling and Analysis. *The Chemical Engineering Journal* **1989**, *40*, 71-82.

715 (14) Liu, L. Molecular Characterisation and Modelling for Refining Processes. University of
716 Manchester, 2015.

717 (15) Mehran Heydari, H. A. a. B. D., Study of Seven-Lump Kinetic Model in the Fluid
718 Catalytic Cracking Unit. *American Journal of Applied Sciences* **7** (1): **2010**, *7* (1), 71-76.

719 (16) Cristina, P., Four – Lump Kinetic Model vs. Three - Lump Kinetic Model for the Fluid
720 Catalytic Cracking Riser Reactor. *Procedia Engineering* **2015**, *100*, 602-608.

- 721 (17) He, P.; Zhu, C.; Ho, T. C., A two-zone model for fluid catalytic cracking riser with
722 multiple feed injectors. *AIChE Journal* **2015**, *61* (2), 610-619.
- 723 (18) Tsuo, Y. P.; Gidaspow, D., Computation of flow patterns in circulating fluidized beds.
724 *A.I.Ch.E.* **1990**, *36*, 885.
- 725 (19) John, Y. M.; Patel, R.; Mujtaba, I. M., Modelling and simulation of an industrial riser in
726 fluid catalytic cracking process. *Computers & Chemical Engineering* **2017**.
- 727 (20) Ellis, R. C.; Li, X.; Riggs, J. B., Modeling and optimization of a model IV fluidized
728 catalytic cracking unit. *AIChE Journal* **1998**, *44* (9), 2068-2079.
- 729 (21) Souza, J. A.; Vargas, J. V. C.; von Meien, O. F.; Martignoni, W. P.; Ordonez, J. C., The
730 inverse methodology of parameter estimation for model adjustment, design, simulation,
731 control and optimization of fluid catalytic cracking (FCC) risers. *Journal of Chemical*
732 *Technology & Biotechnology* **2009**, *84* (3), 343-355.
- 733 (22) León-Becerril, E.; Maya-Yescas, R.; Salazar-Sotelo, D., Effect of modelling pressure
734 gradient in the simulation of industrial FCC risers. *Chemical Engineering Journal* **2004**, *100*
735 (1), 181-186.
- 736 (23) Sadeghbeigi, R., Fluid Catalytic Cracking Handbook. In *An Expert Guide to the*
737 *Practical Operation, Design, and Optimization of FCC Units* [Online] Third Edition ed.; The
738 Boulevard, Langford Lane, Kidlington, Oxford, OX5 1GB, UK: UK, 2012.
- 739 (24) Kasat, R. B.; Kunzru, D.; Saraf, D. N.; Gupta, S. K., Multiobjective Optimization of
740 Industrial FCC Units Using Elitist Nondominated Sorting Genetic Algorithm. *Industrial &*
741 *Engineering Chemistry Research* **2002**, *41* (19), 4765-4776.
- 742 (25) Du, Y.; Zhao, H.; Ma, A.; Yang, C., Equivalent Reactor Network Model for the
743 Modeling of Fluid Catalytic Cracking Riser Reactor. *Industrial & Engineering Chemistry*
744 *Research* **2015**, *54* (35), 8732-8742.
- 745 (26) Souza, J. A.; Vargas, J. V. C.; Von Meien, O. F.; Martignoni, W.; Amico, S. C., A two-
746 dimensional model for simulation, control, and optimization of FCC risers. *AIChE Journal*
747 **2006**, *52* (5), 1895-1905.
- 748 (27) Kalota, S. A.; Rahmim, I. I., Solve the Five Most Common FCC Problems. In *Advances*
749 *in Fluid Catalytic Cracking I. New Orleans.*, Expertech Consulting Inc., Irvine and E-
750 MetaVenture, Inc., Houston: AIChE Spring National Meeting, 2003.
- 751 (28) Ali, H.; Rohani, S., Dynamic Modeling and Simulation of a Riser-Type Fluid Catalytic
752 Cracking Unit. *Chemical Engineering Technology* **1997**, *20*, 118-130.
- 753 (29) Wilson, J. W., *Fluid catalytic cracking technology and operations*. PenWell Pub. Co:
754 Tulsa, OK, 1997.
- 755 (30) Nuhu, M.; Olawale, A. S.; Salahudeen, N.; Yusuf, A. Z.; Mustapha, Y., Exergy and
756 Energy Analysis of Fluid Catalytic Cracking Unit in Kaduna Refining and Petrochemical
757 Company. *International Journal of Chemical Engineering and Applications* **2012**, *3* (6), 441-
758 445.
- 759 (31) Ahari, J. S.; Farshi, A.; Forsat, K., A Mathematical Modeling of the Riser Reactor in
760 Industrial FCC Unit. *Petroleum & Coal* **2008**, *50* (2), 15-24.

761